Witnessing nonstationary and non-Markovian environments with a quantum sensor

John W. Rosenberg,[1] Martín Kuffer,[2,3,4] Inbar Zohar,[1] Rainer Stöhr,[5] Andrej Denisenko,[5] Analia Zwick,[2,3,4] Gonzalo A. Álvarez,[2,3,4,*] and Amit Finkler[1,†]

[1] *Department of Chemical and Biological Physics and AMOS, Weizmann Institute of Science, 7610001 Rehovot, Israel*

[2] *Centro Atómico Bariloche, CONICET, CNEA, 8400 San Carlos de Bariloche, Argentina*

[3] *Instituto de Nanociencia y Nanotecnología, CNEA, CONICET, 8400 San Carlos de Bariloche, Argentina*

[4] *Instituto Balseiro, CNEA, Universidad Nacional de Cuyo, 8400 San Carlos de Bariloche, Argentina*

[5] *3. Physikalisches Institut, Universität Stuttgart, 70569 Stuttgart, Germany*

(Received 16 June 2025; revised 12 October 2025; accepted 19 December 2025; published 21 January 2026)

Quantum sensors offer exceptional sensitivity to nanoscale magnetic field fluctuations, where nonstationary effects—such as spin diffusion—and non-Markovian dynamics arising from coupling to few environmental degrees of freedom play critical roles. Because fully reconstructing the microscopic structure of realistic spin baths is often infeasible, a practical challenge is to identify the dynamical features that are actually encoded in the sensor's decoherence signal. Here we demonstrate how quantum sensors can operationally characterize the statistical nature of environmental noise, distinguishing between stationary and nonstationary behaviors, as well as Markovian and non-Markovian dynamics. Using nitrogen-vacancy centers in diamond as a platform, we develop a physical noise model that captures the essential dynamical features of realistic environments relevant to sensor observables—independently of the microscopic bath details— and provides analytical predictions for Ramsey decay across different regimes. These predictions are experimentally validated through controlled noise injection with tunable correlation properties. Our results showcase the capability of quantum sensors to isolate and identify key dynamical properties of complex environments, without requiring full microscopic bath reconstruction. This work clarifies the operational signatures of nonstationarity and non-Markovian behavior at the nanoscale and lays the foundation for strategies that mitigate decoherence while exploiting environmental dynamics for enhanced quantum sensing.

DOI: 10.1103/13mr-493z

I. INTRODUCTION

Quantum technologies [1–3] rely on preserving quantum coherence for both information processing and sensing. In quantum computing, decoherence from environmental noise limits fidelity and scalability [4–7], making noise characterization essential. In quantum sensing, by contrast, decoherence serves as a resource: the sensor's sensitivity to its environment enables the probing of physical systems via their noise signatures [8,9]. Understanding decoherence is thus key to both mitigating its effects and harnessing it for precision sensing at the nanoscale.

Noise-induced decoherence is ubiquitous in quantum systems, appearing in contexts ranging from nuclear spin baths [10–12] and hyperfine interactions in diamond [13, 14] to quantum dots [15], superconducting qubits [16], and silicon donor defects [17]. Techniques such as dynamical decoupling and quantum error correction have been developed to counteract decoherence [18–22], but their effectiveness relies on detailed knowledge of the noise characteristics [23–30]. Most existing methods, moreover, assume that the noise is stationary—i.e., that its statistical properties do not change in time [24,25,28,31].

At the nanoscale, where quantum sensors such as atomic defects in solids operate [32,33], the sensing radii are typically on the order of 10 nm or less—far below those of conventional magnetic resonance techniques [34–37]. In this regime, environmental dynamics near the sensor, such as spin diffusion, often dominate and exhibit non-Markovian and nonstationary characteristics [38–45]. These features can arise when the environment retains memory of its past or is driven out of equilibrium by local perturbations, respectively. Nonstationarity may originate either intrinsically, from sensor backaction or local perturbations, or may be externally imposed through driven

*Contact author: gonzalo.alvarez@conicet.gov.ar
†Contact author: amit.finkler@weizmann.ac.il

out-of-equilibrium conditions. For example, the act of initializing a quantum sensor—such as optical initialization—can induce a quench, resetting local environmental degrees of freedom and triggering intrinsic nonstationary dynamics due to quantum backaction [40,46]. In contrast, sudden temperature changes, chemical reactions, environmental excitations, or phase transitions can externally drive the bath away from equilibrium [38,39,47,48].

While such behavior complicates efforts to mitigate decoherence in quantum information platforms, it also offers opportunities: the decoherence itself becomes a signal, encoding the statistical properties of the surrounding environment. Quantum sensors therefore offer a powerful platform for probing these complex dynamics. However, unlocking this potential requires systematic frameworks for identifying and distinguishing between different types of environmental noise. Despite their importance, nonstationary [49–53] and non-Markovian [43,54–56] noise processes remain poorly understood and difficult to characterize, limiting progress in both quantum control and nanoscale sensing.

Despite their ubiquity and relevance, there remains no general framework for identifying or classifying the statistical properties of real noise environments at the nanoscale. Each environment—whether biological, solid state, or chemical—has unique microscopic details, making first-principles modeling impractical in most cases. Nevertheless, many such systems share common features, such as memory effects [14,52] or departures from equilibrium [13,38–40,45–48,57]. What is needed are experimentally validated strategies that can isolate and characterize these features independently of system-specific complexity.

While real environments—such as paramagnetic spin baths—are governed by complex quantum many-body dynamics, a quantum sensor interacts with them through effective stochastic magnetic fields. As a result, fully reconstructing the microscopic bath is not only a formidable challenge in realistic settings but also often unnecessary for sensing tasks. Instead, what the sensor provides is partial but highly informative access to the statistical structure of the environment through its decoherence signal. A more practical and experimentally relevant path forward, rather than modeling every microscopic degree of freedom, is first identifying the dynamical features that are operationally encoded in the measured sensor decoherence—such as whether the bath is stationary or out of equilibrium, and whether memory effects are present. Our approach embraces this perspective: rather than aiming for complete bath reconstruction, it focuses on capturing the dynamical properties that directly manifest themselves in the sensor response, providing a classification aligned with experimentally accessible observables.

To this end, we introduce a general model that captures key aspects of realistic noise processes—namely, whether they are stationary or nonstationary, and Markovian or non-Markovian. The model is analytically tractable and allows us to derive closed-form predictions for the Ramsey decay of a quantum sensor coupled to such noise. Crucially, we demonstrate that these four dynamical regimes (stationary Markovian, stationary non-Markovian, quenched Markovian, and quenched non-Markovian) exhibit qualitatively distinct signatures in the short-time and long-time behavior of the sensor signal. This enables us to classify the dynamical nature of an environment directly from the Ramsey response, without assuming prior knowledge of the full noise correlation functions.

The model reduces to the well-known Ornstein-Uhlenbeck (OU) process in the Markovian limit, but can capture non-Markovian statistical features essential to quantum sensing. As a Gaussian model, it can also be viewed as a particular case of a Caldeira-Legget (CL) bath. However, while CL baths may exhibit arbitrary spectral densities and are typically analyzed at equilibrium, our framework focuses on the physically motivated subset that remains analytically tractable yet rich enough to capture out-of-equilibrium and non-Markovian dynamics. This makes it ideally suited to classify stationary versus nonstationary and Markovian versus non-Markovian regimes in quantum sensing scenarios.

We validate these predictions using a single nitrogen-vacancy (N-V) center in diamond as a quantum sensor. Rather than relying on an uncontrolled physical bath, we emulate the statistical structure of the model environments through injected noise with tunable parameters. This level of control allows us to isolate dynamical features—the impact of memory, damping, and initial-state quenches on the Ramsey decay—that would coexist in a real spin bath, making the approach a proof-of-principle demonstration of what a quantum sensor can, in practice, identify about its environment. We find strong agreement between experimental measurements and theoretical predictions, confirming that a quantum sensor can act as a witness of the environmental noise's statistical nature.

By establishing a pathway to disentangle and identify non-Markovian and nonstationary features, our work opens new directions for nanoscale noise characterization. Beyond offering a robust foundation for quantum sensing in complex environments, the results also have direct implications for improving decoherence control in quantum technologies, where understanding the nature of noise is a prerequisite for its mitigation [49–56]. We emphasize that the framework is designed to classify and identify dynamical regimes rather than to reconstruct the full microscopic structure of arbitrary baths—a task that generally requires additional complementary spectroscopy techniques [52]. The present approach therefore provides a practical foundation for interpreting the decoherence signatures observed in realistic sensing scenarios.

II. ANALYTICAL FRAMEWORK FOR QUANTUM SENSING OF STATIONARY AND NONSTATIONARY, MARKOVIAN AND NON-MARKOVIAN NOISE

A. The N-V quantum sensor

The N-V quantum sensor is a spin-1 defect that detects the axial component (with respect to the N $\rightarrow$ V axis) $B_z(t) = B_0 + \Delta B_z(t)$ of a magnetic field through its Zeeman interaction [Fig. 1(a)]. By considering a fluctuating field along the N $\rightarrow$ V axis, we remain within the framework of pure dephasing and ignore other relaxation processes. This approximation is well-justified whenever the total measurement duration is much shorter than the longitudinal relaxation time T_1 of the N-V center. We use two spin substates, $|0\rangle$ and $|-1\rangle$, to form the qubit [58]. By preparation of a superposition of these states, the relative phase accumulated between them over time reflects the magnetic field fluctuations. Application of microwave (MW) pulses at the qubit's Larmor frequency allows one to use the rotating-wave approximation, where the stationary term $\gamma_{\text{N-}V}B_0 t$ is canceled, and where $\gamma_{\text{N-}V}$ is the gyromagnetic ratio of the N-V center. The accumulated phase is then given by $\varphi(t) = \int_0^t \gamma_{\text{N-}V}\Delta B_z(t')dt'$, and the measured fluorescence will be proportional to the difference between the qubit state projections onto $|0\rangle$ and onto $|-1\rangle$, which will oscillate as $\cos\left(\int_0^t \gamma_{\text{N-}V}\Delta B_z(t')dt'\right)$. For more details, see Appendix E 6.

When the environment induces pure dephasing and the noise is Gaussian, the semiclassical approximation becomes exact: the effect of the environment—even if quantum in nature—can be fully described by a classical stochastic process $n(t)$ [59]. This applies to a broad class of physical systems, including spin baths and bosonic environments under weak coupling to the sensor [12–14,25,26,28]. Modeling $n(t)$ as a Gaussian process is therefore both physically justified and analytically advantageous: It captures essential features of non-Markovian and nonstationary noise, as we show below, while avoiding

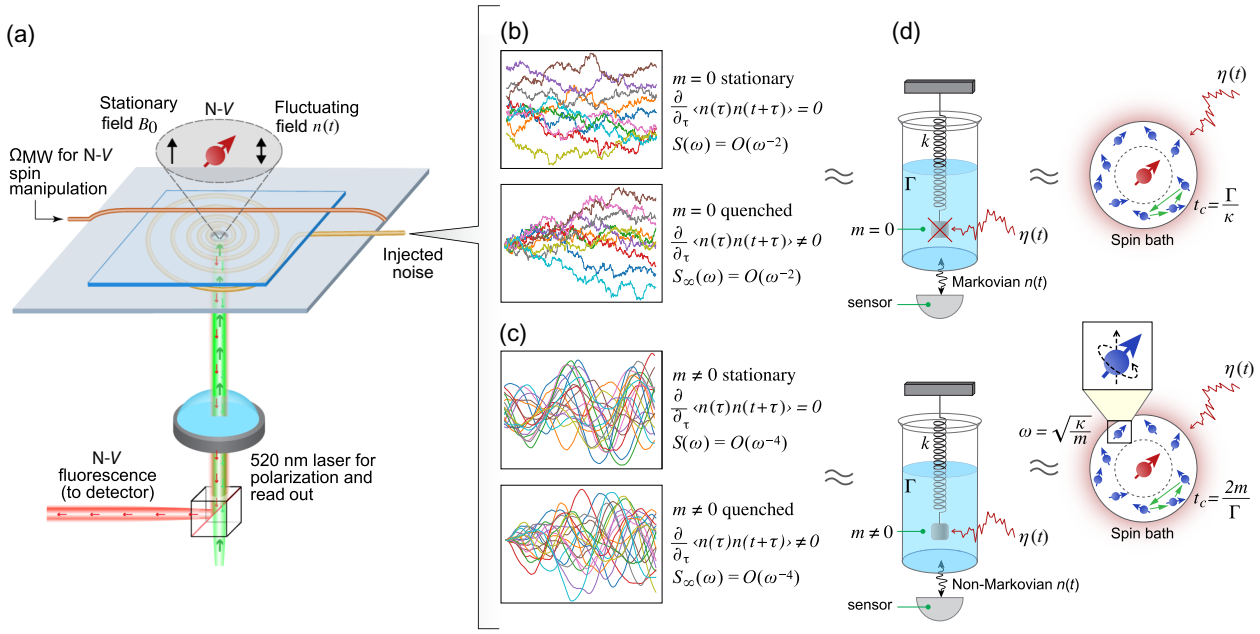

FIG. 1. Experimental setup to probe environmental noise using a single N-V center as a quantum sensor via Ramsey decay measurements. (a) The setup consists of a diamond membrane containing nanopillars with single N-V centers placed on a printed circuit board. The beam from a 520 nm laser is focused through a hole in the board to initialize and read out the N-V spin state. The N-V center is subjected to a stationary magnetic field $B_0 = 298$ G, while environmental field fluctuations $n(t) = \gamma_{\text{N-}V}\Delta B_z(t)$ are generated by injection of noise through a spiral antenna beneath the diamond via a variable voltage. Radio-frequency pulses for N-V spin manipulation are applied via a copper wire above the diamond membrane. (b),(c) Representative samples (ten sample trajectories shown as colored curves for each) of the four noise processes $n(t)$ considered in this study: stationary Markovian noise, quenched Markovian noise, stationary non-Markovian noise, and quenched non-Markovian noise (from top to bottom). We distinguish between Markovian noise [(b), $m = 0$] and non-Markovian noise [(c), $m \neq 0$]. (d) Schematic representation of how magnetic field fluctuations $n(t)$, sensed by the quantum sensor, are modeled as the position of a stochastically driven harmonic oscillator by a Langevin-type equation: $mn'' + \Gamma n' + \kappa n = \eta(t)$. The parameters m, Γ, and κ describe the effective dynamics of the spins that directly couple to the qubit, capturing the oscillatory (non-Markovian) and purely relaxational (Markovian) regimes. The stochastic force $\eta(t)$, illustrated by the red arrow, represents the influence of more distant environmental spins that do not couple directly to the sensor but modulate the collective spin-bath dynamics. This model unifies non-Markovian and Markovian spin-bath behaviors within a single physical framework.

the added complexity of higher-order cumulants. Gaussian noise also provides a paradigmatic and sufficient case for developing the classification framework. Moreover, the qualitative behaviors we identify—such as short-time scaling laws associated with the different regimes and oscillatory correlations signaling non-Markovianity—are expected to remain valid beyond the Gaussian limit, for instance, in nonlinear Langevin-type dynamics that generate non-Gaussian statistics. This provides a general and tractable framework for identifying signatures of complex environmental dynamics through quantum sensors.

We calculate the Ramsey $S(t)$ by averaging the qubit state projection onto $|0\rangle$ over all noise trajectories [see Figs. 1(b) and 1(c)]. Since $n(t)$ is a Gaussian process with mean zero, $\varphi(t)$ is also Gaussian with mean zero and variance σ_t^2. This leads to a signal decay of the form

$$S(t) = \langle \cos(\varphi(t)) \rangle = \int_{-\infty}^{\infty} \frac{1}{\sigma_t \sqrt{2\pi}} e^{-\frac{\varphi^2}{2\sigma_t{}^2}} e^{i\varphi} d\varphi = e^{-\frac{\sigma_t{}^2}{2}}. \tag{1}$$

The correlation function $\langle n(t_1) n(t_2) \rangle$ of the environmental noise evaluated at two different times t_1 and t_2 dictates the attenuation factor

$$\chi(t) = \frac{\sigma_t{}^2}{2} = \int_0^t \int_0^{t_1} \langle n(t_1)\, n(t_2) \rangle \, dt_2 dt_1, \tag{2}$$

providing an exact expression for the Ramsey decay $S(t) = e^{-\chi(t)}$. In real experiments, additional sources of dephasing or relaxation may superimpose an extra exponential envelope on the Ramsey signal. Our framework therefore establishes a baseline scenario that isolates the contribution of the target environment from other noise channels. The predicted signatures remain observable as long as the corresponding decay rates are not dominant over those of the environment under study.

B. Environmental fluctuation model

To capture essential features of non-Markovian and nonstationary environmental noise affecting the qubit, we introduce a general model for the fluctuating magnetic field using a semiclassical stochastic noise process $n(t)$. Rather than targeting a specific microscopic system, this approach aims to reproduce universal statistical behaviors—such as memory effects and out-of-equilibrium evolution—that are expected in realistic quantum environments at the nanoscale.

The temporal correlations of $n(t)$ are described by a Langevin-type equation:

$$m n'' + \Gamma n' + \kappa n = \eta(t), \tag{3}$$

where m denotes an effective mass, quantifying the inertia of the fluctuating field, Γ is a damping coefficient, and κ corresponds to a potential confining the fluctuations [Fig. 1(d)]. The stochastic driving term $\eta(t)$ represents a Gaussian white noise process with zero mean and autocorrelation

$$\langle \eta(t_1)\, \eta(t_2) \rangle = A \delta(t_1 - t_2), \tag{4}$$

capturing random forces with strength A from remote environmental degrees of freedom that do not directly interact with the sensor.

This model is physically grounded and versatile: as we show in Appendix D, it captures the dynamics of diverse systems, including a quantum harmonic oscillator coupled to thermal baths (e.g., Caldeira-Leggett-type models), and spin baths with varying internal couplings, as shown in Fig. 1(d). The parameters m, Γ, and κ encode the properties of environmental modes that interact with the qubit, capturing an interplay between oscillatory and relaxation dynamics. Note that m may coincide with a physical mass, as in the damped harmonic oscillator case (Appendix D 1), or may act as an effective parameter encapsulating multiple physical quantities that determine the inertia of the fluctuating field, as in a spin bath (Appendix D 3). The term $\eta(t)$ accounts for stochastic influences from remote or indirectly coupled environmental degrees of freedom.

A critical feature of this model is the *inertia term*: for $m \neq 0$, the environmental dynamics acquire memory, with future fluctuations depending on past velocities and positions. This generates time-correlated, non-Markovian noise with continuous derivatives [52]. In the limit $m = 0$, the dynamics reduce to an overdamped OU process—fully memoryless and Markovian. When $m \neq 0$, the inertia term introduces a finite memory time, enabling transitions from purely Markovian to non-Markovian behavior. This parameter thus governs the degree of temporal correlations in the noise.

In quantum sensing, the objective is to extract the dynamical properties of the environment itself from the sensor's response. This differs from approaches that focus on classifying the non-Markovianity of the sensor's reduced dynamics [60]. Here we distinguish whether the environmental fluctuations $n(t)$ are Markovian or non-Markovian—on the basis of the presence ($m \neq 0$) or absence ($m = 0$) of memory in their dynamics.

The model also distinguishes between *stationary* and *nonstationary* noise on the basis of initial conditions (Appendix A). Equilibrium states yield stationary noise with correlation functions invariant under time translation, while out-of-equilibrium initialization—such as from quantum backaction—induces nonstationary noise with time-dependent correlation functions. This is particularly relevant for quantum sensors, where initialization perturbs the environment [40,46]. When the noise is stationary, our model corresponds to a Gaussian limit that can be formally mapped to a CL bath with an appropriate spectral

density. However, out-of-equilibrium initial conditions are naturally incorporated within our framework, whereas general CL formulations typically assume equilibrium environments and require additional assumptions to describe quenched or time-dependent states.

Together, the inertia parameter m and the initial conditions of the bath define the four fundamental regimes analyzed in this work: stationary and nonstationary, Markovian and non-Markovian. Each regime produces distinct Ramsey decay signatures, enabling the quantum sensor to diagnose the underlying noise statistics. This framework thus provides a tractable and physically grounded basis for modeling noise-driven decoherence: it admits analytical treatment, enabling systematic investigation of how different environmental dynamics—and their interplay—manifest themselves in the sensor's response.

Our approach is agnostic to bath details, focusing on detecting nonstationary and non-Markovian behavior. We use a simple model to capture essential environmental characteristics, while remaining analytically tractable and allowing us to isolate specific dynamical features (nonstationarity and non-Markovianity). This enables the detection of these specific features without the need to fully characterize the noise spectrum/correlation function of the environment. Our results do not provide a full reconstruction of the environmental noise characteristics, as noise spectroscopy would. Instead, our method uses fewer resources to extract key information from the environmental behavior. Extensions to fully quantum, non-Gaussian, and other more complex environments are possible, but fall beyond the scope of this work.

C. Noise correlation characteristics

The correlation function of environmental noise, which defines the statistical behavior of $n(t)$, determines the Ramsey decay and allows us to distinguish between different types of noise. We examine two limits of the unified stochastic model: Markovian ($m \to 0$) and underdamped non-Markovian ($4\kappa m > \Gamma^2$).

For $m = 0$, representing extremely overdamped systems, the noise behaves as constrained Brownian motion, described by $n' + t_c^{-1} n = \eta(t)/\Gamma$, where $t_c = \Gamma/\kappa$ is the self-correlation time of the environmental fluctuations for the $m = 0$ case, which determines the characteristic timescale over which the environment reaches its equilibrium (stationary) state. This is Markovian noise, with a propagator that lacks memory of previous states.

For $m \neq 0$, which we use to represent underdamped systems, the noise behaves as a stochastically driven damped harmonic oscillator: $n'' + 2t_c^{-1} n' + \omega_0^2 n = \eta(t)/m$, where $t_c = 2m/\Gamma$ is the self-correlation time for the $m \neq 0$ case, and $\omega_0 = \sqrt{\kappa/m}$ is the restoring frequency. This same equation also describes overdamped systems. In these cases, oscillations are suppressed and the self-correlation function decays biexponentially, as observed for nuclear spin baths under strong dephasing [61,62]. Such dynamics still exhibit non-Markovian memory due to the coexistence of two distinct relaxation rates, which cannot be reproduced by a purely Markovian Ornstein-Uhlenbeck process.

The inertia term ($m \neq 0$) introduces an additional timescale ω_0 such that the coexistence of ω_0 and t_c couples the dynamics to past velocities and positions, thereby generating non-Markovian memory effects. In the underdamped regime ($\omega_0 t_c > 1$), the resulting oscillatory correlations with effective frequency $\Omega = \sqrt{\omega_0^2 - t_c^{-2}}$ are a hallmark of many non-Markovian processes (derivations are provided in Appendix A 2).

This model effectively captures the behavior of spin baths with randomly interacting spins, where the correlation function exhibits a dynamical phase transition between overdamped and underdamped behavior depending on the structure of the environmental Hamiltonian. Such dynamics are beyond the scope of Markovian descriptions [39]. It also applies to other relevant quantum environments, including thermally populated bosonic modes and quantum spin systems (Appendix D).

For a nuclear spin bath, for example, ω_0 corresponds to the Larmor frequency, and t_c denotes the spin decoherence time, as depicted in Fig. 1(d). In our experiments, we focus on the case $\omega_0 t_c > 1$ of underdamped dynamics, where the noise simultaneously oscillates and relaxes toward equilibrium, with effective frequency $\Omega = \sqrt{\omega_0^2 - t_c^{-2}}$.

Both Markovian noise and non-Markovian noise may exhibit stationary or nonstationary behavior, depending on the initial state. The latter arises when the environment is initialized out of equilibrium—either via an external quench due to driven out-of-equilibrium phenomena, or through intrinsic quantum backaction from sensor initialization [40,46].

The quantum sensor's sensitivity to these noise characteristics enables it to act as a witness to nonstationary and/or non-Markovian behavior. Figure 1(b) illustrates differences in correlation function behavior for the primary noise types. For stationary noise, the correlation function is time translation invariant, $\langle n(t_1) n(t_2)\rangle = \langle n(0) n(\Delta t)\rangle$, where $\Delta t = t_2 - t_1$. For nonstationary noise, $\langle n(t_1) n(t_2)\rangle$ depends on both t_1 and t_2.

For Markovian noise, the spectral density $S_\infty(\omega) \propto 1/(1 + t_c^2 \omega^2)$, defined as the Fourier transform of $\lim_{t_1 \to \infty} \langle n(t_1) n(t_1 + \Delta t)\rangle$, has a Lorentzian shape, i.e., is the inverse of an even quadratic polynomial in ω, with noise fluctuations having discontinuous time derivatives. For non-Markovian noise ($m \neq 0$), $S_\infty(\omega) \propto 1/((\omega^2 - \omega_0^2)^2 + 4t_c^{-2}\omega^2)$ is the inverse of an even quartic polynomial, with continuity in noise derivatives. For our non-Markovian measurements, we focus on an underdamped regime where $S_\infty(\omega)$ peaks at $\pm\sqrt{\Omega^2 - t_c^{-2}}$ (or at

0 if $\Omega t_c < 1$). Detailed derivations of the correlation function $\langle n(t_1)n(t_2)\rangle$ and the Ramsey decay attenuation factor $\chi(t)$ are provided in Appendixes A and B, respectively, for all the noise types considered, and derivations of $S_\infty(\omega)$ for Markovian and underdamped noise are provided in Appendix C.

D. Ramsey decay for stationary and nonstationary Markovian noise

The differences between stationary and nonstationary Markovian noise are evident in the short-time behavior of the Ramsey decay $\chi(t)$. For stationary (equilibrium) Markovian noise, the leading-order term in the Ramsey decay is expressed as $\chi(t) \approx (\Delta^2/2)t^2 + O(t^3)$. Note that it is proportional to t^2 and depends only on the equilibrium variance $\Delta^2 = \lim_{t\to\infty}\langle n(t)^2\rangle$, and not on the correlation time t_c. In contrast, for quenched (nonstationary, with an initial condition $n_0 = 0$) Markovian noise, the attenuation factor is expressed as $\chi(t) \approx (\Delta^2/3t_c)t^3 + O(t^4)$, depending on both t_c and Δ^2. Alternatively, the attenuation factor can also be written as $\chi(t) \approx \frac{2}{3}(A/\Gamma^2)t^3 + O(t^4)$, where we can see that the leading order of the decay factor of the quenched Markovian noise depends only on the normalized driving strength for the Markovian process A/Γ^2. For further details, see Appendix B 1.

This indicates that, for short times and sufficiently large values of t_c, the ratio between the Ramsey signals for quenched Markovian noise versus equilibrium Markovian noise can become significantly large, allowing clear differentiation between the two. Additionally, the Ramsey signal can serve as a witness of various nonstationary noise effects, such as identifying the moment of a quench relative to the start time of the Ramsey measurement or detecting abrupt changes in correlation time.

In the short-time regime, quenched noise induces a slower Ramsey decay—of higher order in time—compared with equilibrium noise, underscoring the potential of Ramsey interferometry to distinguish between different noise types. In practice, the short-time scaling can be resolved provided that the bath correlation time exceeds the control pulse duration—a condition typically satisfied in N-V center experiments.

At long times, both stationary noise and nonstationary noise—whether Markovian ($m = 0$) or non-Markovian ($m \neq 0$)—exhibit attenuation factors that converge to the same decay rate. This shows that long measurement times are less efficient at detecting early-time nonstationary dynamics than measurement times that are smaller or approximately equal to t_c. However, the curves remain offset by a constant shift, reflecting residual information from the initial nonstationary state (see Appendix B 1 for the derivation and Table III in Appendix B 3). This demonstrates that memory of the early-time dynamics is retained even after the environment has relaxed to stationarity.

These distinct short-time and long-time dependencies also imply that the parameters t_c, A/Γ^2, and Δ^2 affect different measurable aspects of the Ramsey response. At short times, the decay depends only on Δ^2 for equilibrium noise and on A/Γ^2 for quenched noise, while t_c governs the crossover between these regimes and the long-time offset. Consequently, a single measurement restricted to one regime cannot determine all parameters independently. However, a combination of stationary and quenched experiments enables the unambiguous determination of these parameters. This principle is analyzed quantitatively in Appendix H.

E. Ramsey decay as a witness of non-Markovian noise: stationary versus nonstationary

The signatures of non-Markovian noise sources in Ramsey decay reveal a richer array of phenomena compared with their Markovian counterparts. Here we focus on underdamped non-Markovian ($m \neq 0$) noise. Sample plots of the analytical expressions for Ramsey decay curves for equilibrium and quenched underdamped non-Markovian noise are shown in Fig. 5 in Appendix B 4.

For equilibrium (stationary) noise, the leading-order term of the Ramsey attenuation factor (see Appendix B 2 for the derivation and Table III in Appendix B 3) is written as $\chi(t) \approx (\Delta^2/2)t^2 + O(t^3)$. Note that the leading order coincides with the result for the stationary Markovian case. As before, the result depends only on the equilibrium variance Δ^2 and is of order t^2. Note as well how this means that short-time ($t < \Omega^{-1}, t_c$) Ramsey spectroscopy cannot distinguish between Markovian noise and non-Markovian noise when measuring them in a stationary state. This is intuitive, since (non-)Markovianity is a dynamical property, and thus the differences it induces can be sensed only after enough time has passed for the state of the noise to evolve. This result also holds in the overdamped regime, where the absence of oscillations does not alter the leading short-time t^2 scaling of $\chi(t)$.

In contrast, for quenched (nonstationary, with initial conditions $n(0) = n'(0) = 0$) underdamped non-Markovian ($m \neq 0$) noise, the leading order of the attenuation factor is expressed as $\chi(t) \approx \Delta^2(\omega_0{}^2/10t_c)t^5 + O(t^6)$. Here the behavior changes significantly: it is of order t^5, and depends not only on the equilibrium variance Δ^2 but also on the self-correlation time t_c and the oscillation frequency Ω. This marks a clear departure from the quenched Markovian case. Thus, one can infer that short-time Ramsey experiments can indeed distinguish between Markovian and non-Markovian environments, provided the proper quench is induced in these environments before the measurement. For further details and the derivation, see Appendix B 2 and Table III in Appendix B 3.

This distinction is particularly relevant because it allows the ratio of Ramsey signals (quenched versus equilibrium)

under underdamped non-Markovian noise to become arbitrarily large at short times ($t < \Omega^{-1}, t_c$), given sufficiently large t_c and small ω_0. This suggests that short-time Ramsey measurements can effectively discriminate between stationary and nonstationary non-Markovian noise.

Finally, the attenuation factor can be expanded at short times as $\chi(t) \approx (A/40m^2)t^5 + O(t^6)$, where the t^5 term represents the leading-order contribution for quenched non-Markovian noise with initial conditions $n(0) = n'(0) = 0$. This leading-order coefficient depends only on the normalized driving strength A/m^2, while the influence of other bath parameters, such as t_c and ω_0, appears only in higher-order terms ($\mathcal{O}(t^6)$ and beyond). The suppression of lower-order contributions is a direct consequence of the quench, which resets the bath away from equilibrium. The full expression for $\chi(t)$, including all parameter dependencies, is derived in Appendix B 2. We note that the same leading-order independence from other bath parameters also holds in the overdamped regime.

For both non-Markovian noise and Markovian noise, reducing the damping (i.e., increasing t_c) causes the quenched Ramsey decay curve to slow down at short times ($t \ll t_c$) relative to the equilibrium Ramsey decay curve. However, the oscillatory nature of $\chi(t)$ for underdamped non-Markovian noise introduces a striking difference between the Ramsey signals for quenched noise versus equilibrium noise. Specifically, for equilibrium underdamped non-Markovian noise with large t_c, the Ramsey signal exhibits collapses and revivals, as shown in Fig. 5 in Appendix B 4: the signal decays nearly completely, only to revive periodically, forming peaks at $t = 2\pi m/\Omega$ for $m \in \mathbb{Z}^*$ ($\mathbb{Z}^*$ denoting the positive integers), where $\Omega = \sqrt{\omega_0{}^2 - t_c^{-2}}$ is the effective oscillation frequency of the environment.

In contrast, quenched underdamped non-Markovian noise does not produce the collapses and revivals seen in the stationary case (Fig. 5 in Appendix B 4). Instead, the Ramsey signal exhibits plateaus at $t = 2\pi m/\Omega$ for $m \in \mathbb{Z}^*$, with the steepest decay near $t = \pi(2m+1)/\Omega$. Despite the underlying memory, nonstationarity suppresses coherent revivals, replacing them with delayed decoherence and flat intervals—revealing how initial conditions critically shape non-Markovian dynamics.

These contrasting behaviors also illustrate how different dynamical features of the Ramsey response encode distinct environmental parameters. The oscillation frequency ω_0 determines the revival period, the correlation time t_c sets the envelope and plateau widths, and the overall noise strength A/m^2 controls the decay rate at short times. Consequently, a single stationary or quenched experiment samples only a subset of this information, and fitting all parameters independently may not result in a unique optimal fit due to high dependency between the parameters if the accessible timescales are limited. By combining stationary and quenched measurements—each sensitive to different physical features—one gains access to independent observables that together allow ω_0, t_c, and A/m^2 to be extracted unambiguously. This principle is discussed in more detail in Appendix H.

The origin of collapses and revivals for equilibrium underdamped non-Markovian noise lies in a noise variance that is constant in time and the sharp peak in its noise spectrum near the oscillation frequency, at $\pm\sqrt{\Omega^2 - t_c^{-2}}$. This peak induces periodic cancellations of noise correlations and anticorrelations, producing revivals in the Ramsey signal at integer multiples of $2\pi/\Omega$. Such behavior cannot be seen with Markovian noise sources, where the correlation function is strictly non-negative, thus precluding the possibility of collapses and revivals. Therefore, the presence of these revivals in the equilibrium Ramsey signal serves as a robust witness of non-Markovianity in the noise source.

Additionally, this model indicates another way in which Ramsey measurements can reveal out-of-equilibrium dynamics: As the starting time of the Ramsey measurement approaches a quench, the curvature of the Ramsey signal at revival points approaches zero, providing a distinct indicator of the transition to nonstationary noise. Thus, Ramsey measurements can serve as powerful tools for identifying both non-Markovian behavior and of out-of-equilibrium dynamics in complex noise environments.

III. EXPERIMENTAL DEMONSTRATION OF QUANTUM SENSING OF NONSTATIONARY AND NON-MARKOVIAN NOISE

A. Experimental implementation

To test our theoretical predictions, we perform Ramsey measurements on a single N-V center under injected noise with tunable correlation functions. Details of the noise generation algorithms and their validation against target correlation functions are provided in Appendixes E and F. While real environments are complex and system-specific, synthetic noise offers a controlled platform to isolate and probe key statistical features—such as nonstationarity and memory—relevant to nanoscale quantum sensing.

We use a diamond pillar containing a single N-V center, with a sufficiently long T_2^* time to ensure that the injected noise dominates the sensor's decoherence. We manipulate the state of the N-V center using radio-frequency pulses generated by a wire passing above the diamond wafer, and we generate the injected noise by applying a voltage with the desired correlation function to a spiral antenna located beneath the diamond [see Fig. 1(a)]. We use a confocal fluorescence microscope to focus a 520 nm laser on the N-V center for initialization and readout. For each time point in each Ramsey decay curve, we collect photons for 100 realizations of the injected noise, so that the projections of the N-V state onto $|0\rangle$ are sensitive to the

full statistical distribution of the noise realizations (see Appendix E).

B. N-V characterization

Optically detected magnetic resonance (ODMR), Rabi, and Ramsey measurements for this N-V center are shown in Fig. 6 in Appendix E 3. To account for imperfections in the drift correction, we also perform drift-corrected Ramsey measurements with 0 V injected noise as a control and compare the results with a drift-corrected Ramsey measurement where a constant 0.45 V is applied to the spiral. The results of these control measurements are also shown in Appendix E 3. The Ramsey signal from the latter experiment shows an oscillation at 3.6 MHz, which is significantly faster than the decay rate of 0.608 μs^{-1}, indicating that this N-V center is suitable for sensing the injected noise.

C. Probing stationary versus nonstationary Markovian noise

In the first set of injected noise measurements, we examine the effect of equilibrium Markovian noise and quenched Markovian noise with standard deviation $\Delta = 0.10$ V at equilibrium and correlation times t_c of 10, 5, 2.5, and 1.25 μs. Figure 2 shows the Ramsey decays, along with fits using the analytical expressions for Ramsey decay

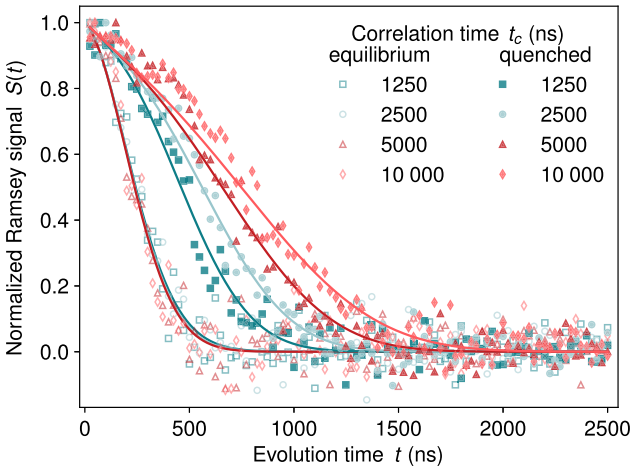

FIG. 2. Ramsey decay signals $S(t)$ for equilibrium and quenched Markovian noise, with correlation times t_c of 1.25, 2.5, 5, and 10 μs, and noise standard deviation $\Delta = 0.10$ V. Symbols represent experimental data; solid curves are analytical fits using t_c as a free parameter, consistent with the injected values. For equilibrium noise, all curves collapse onto a single decay due to identical short-time behavior, making them visually indistinguishable. In contrast, quenched noise curves remain clearly distinct, demonstrating the Ramsey signal's sensitivity to the correlation time in nonstationary regimes.

for equilibrium Markovian noise and quenched Markovian noise shown in Eqs. (B1) and (B3).

One can see that the analytical expressions for equilibrium Markovian noise and quenched Markovian noise provide excellent fits for the experimental data.

Notably, our results follow the short-time behavior predicted by the model, and they demonstrate that information about the correlation time can be extracted from a quenched environment—but not from an equilibrium environment—if the coupling with the environment is strong enough that stationary noise causes the Ramsey signal to decay significantly on a timescale shorter than the correlation time.

The contrast between equilibrium Markovian noise and quenched Markovian noise is most evident at short evolution times. For equilibrium noise, the Ramsey signal decays significantly at times much shorter than the correlation time t_c and then reaches the noise floor, such that the decay curves for different t_c values overlap. In contrast, in a quenched environment, the correlation time can be inferred before the signal significantly decays, increasing the signal-to-noise ratio for estimating the correlation time. Figure 2 illustrates how the Ramsey decay curves for Markovian noise with different t_c values remain distinct in the quenched case. Details of the fitting procedure used to extract Δ and t_c are provided in Appendix H. It is important to note that when a measurement probes only a restricted dynamical regime, the fitting parameters may become correlated, leading to overparametrization. This is a universal feature of time-domain spectroscopy rather than a limitation of our model: if the measurement window does not encompass the relevant timescales, not all environmental parameters can be independently extracted. In our case, the equilibrium Ramsey experiment is sensitive mainly to the stationary variance Δ^2, while the quenched Ramsey experiment isolates the driving strength A/Γ^2. By jointly analyzing both, one gains access to independent observables that together determine all relevant parameters of the noise, thereby resolving the apparent parameter correlations. This principle is analyzed in Appendix H.

To further demonstrate the utility of quantum sensors in extracting dynamical parameters from out-of-equilibrium environments, we investigated whether the timing of a quench can be inferred from the sensor response. Specifically, we measured Ramsey signals for both quenched Markovian noise and equilibrium Markovian noise with standard deviation $\Delta = 0.10$ V at equilibrium and correlation time $t_c = 10$ μs, and then introduced controlled delays t_d of 250, 625, 1250, and 2500 ns between the quench and the start of the Ramsey measurement. The resulting signals are shown in Fig. 3(a), along with fits using the analytical expression for the Ramsey signal of Markovian noise with a delayed quench derived in Eq. (B5), with the quench parameter $Q = e^{\frac{-2t_d}{t_c}}$ as a free parameter in the fit.

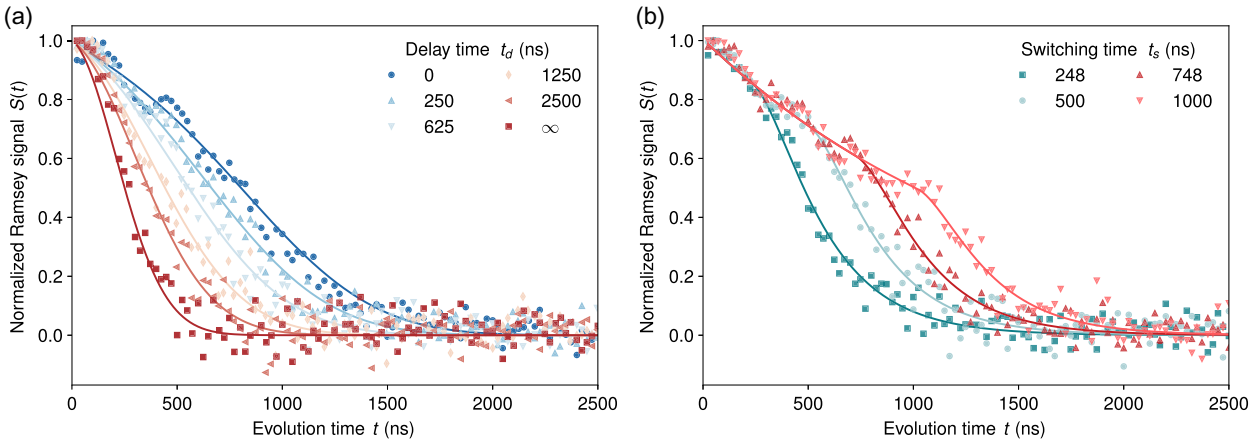

FIG. 3. Measured Ramsey signals $S(t)$ used to probe the onset of quenches in Markovian noise environments. Symbols represent experimental data and solid lines are fits to the analytical expressions. (a) Ramsey decays for noise with standard deviation $\Delta = 0.10$ V and correlation time $t_c = 10$ μs measured at equilibrium ($t_d = \infty$) and with quenches occurring at delays t_d of 0, 250, 625, 1250, and 2500 ns before the start of the Ramsey sequence. (b) Ramsey decays for noise with fixed standard deviation $\Delta = 0.10$ V and a correlation time that switches from $t_a = 15$ ns to $t_b = 150$ ns at times t_s of 248, 500, 748, and 1000 ns.

The delay times t_d extracted from the fits are shown in Table I, and match the known delay times used to generate the injected noise. These results confirm that, when the correlation time is known, the N-V sensor's Ramsey response can be used to determine when a quench occurred.

The Ramsey signal from a N-V center can also be used to determine when an abrupt switch in correlation time occurred relative to the start of the measurement. In a physical system, such a switch could arise, for example, from an abrupt change in temperature that changes the rate of molecular tumbling. To demonstrate this, we measured Ramsey signals for equilibrium Markovian noise with a constant standard deviation $\Delta = 0.10$ V and a correlation time that switches from $t_c = t_a = 15$ ns to $t_c = t_b = 150$ ns at switching times t_s of 248, 500, 748, and 1000 ns after the start of the measurement. The results are shown in Fig. 3(b), along with fits using the analytical expression for the Ramsey signal under equilibrium Markovian noise with a switched correlation time, shown in Appendix B 1 [Eqs. (B7) and (B8)]. The time of the switch relative to the start of the measurement was used as a free fitting parameter. The switching times extracted from the fits are summarized in Table I, and show good agreement with the known switching times used to generate the injected noise. Another example of switching time detection can be found in Appendix G.

D. Probing stationary versus nonstationary non-Markovian noise

Lastly, we examine the effect of injected underdamped equilibrium non-Markovian ($m \neq 0$) noise. Figure 4(a) shows the Ramsey signals measured upon injection of equilibrium non-Markovian noise with an effective driving strength A/m^2 of 0.054 $V^2/\mu s^3$, a damping coefficient $2{t_c}^{-1}$ of 0.1 MHz, and restoring frequencies ω_0 of 5, 6, and 7 MHz, along with fits using the analytical expressions for Ramsey decay under underdamped non-Markovian noise shown in Eqs. (B10), (B12). As expected, the observed Ramsey decay curves oscillate with effective frequency $\Omega = \sqrt{\omega_0^2 - t_c^{-2}}$, so increasing the restoring frequency leads to earlier occurrence of the first revival.

Figure 4(b) shows Ramsey signals measured upon injection of equilibrium non-Markovian noise with the same effective driving strength A/m^2 of 0.054 $V^2/\mu s^3$, restoring frequency $\omega_0 = 6$ MHz, and damping coefficients $2{t_c}^{-1}$ of 0.025, 0.05, 0.1, 0.15, and 0.2 MHz, along with corresponding analytical fits. For comparison, these damping coefficients are similar to values of ${T_2}^{-1}$ obtained for the P1 spin bath in nitrogen-doped diamond [14]. As expected, increasing the damping coefficient reduces the amplitude of the collapse and revival features and broadens the revival peak. Importantly, if ω_0 represents a bare

TABLE I. Comparison of the delay times t_d and switching times t_s extracted from fitting the Ramsey signals in Fig. 3 with the analytical expressions vs. the known values of the delay times and switching times for the injected noise.

Injected delay time t_d (ns)	250	625	1250	2500
Fitted delay time t_d (ns)	271 ± 30	641 ± 48	1418 ± 96	2662 ± 198
Injected switching time t_s (ns)	248	500	748	1000
Fitted switching time t_s(ns)	235 ± 13	504 ± 15	728 ± 17	1017 ± 20

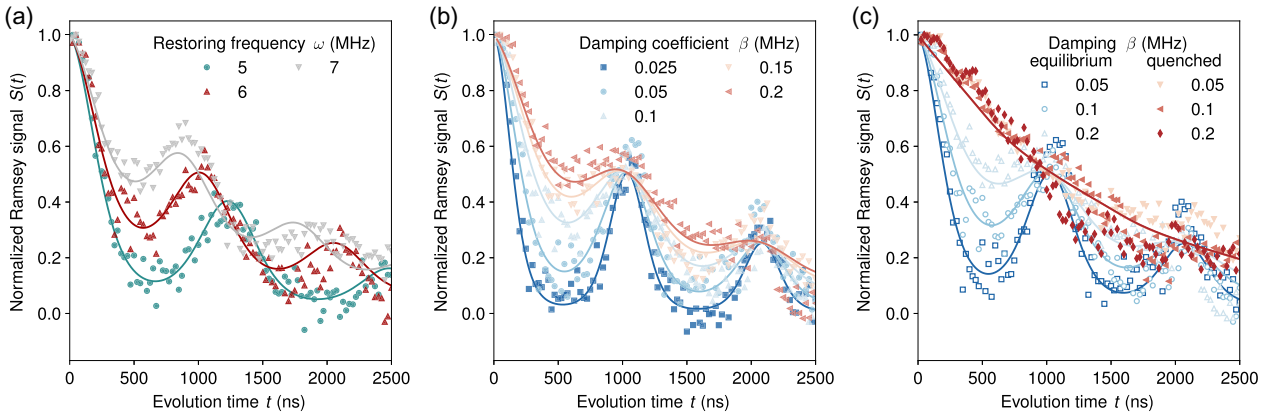

FIG. 4. Measured Ramsey decay signals $S(t)$ under equilibrium and quenched underdamped non-Markovian noise ($m \neq 0$) used to probe non-Markovian features and their interplay with nonstationary effects. The effective driving strength is fixed at $A/m^2 = 0.054\ \mathrm{V}^2/\mu\mathrm{s}^3$. (a) Ramsey signals for a fixed damping coefficient $2t_c^{-1} = 0.1$ MHz, and restoring frequencies ω_0 of 5, 6, and 7 MHz. (b) Ramsey signals for a fixed restoring frequency $\omega_0 = 6$ MHz and damping coefficients $2t_c^{-1}$ of 0.025, 0.05, 0.1, 0.15, and 0.2 MHz. (c) Comparison of equilibrium and quenched non-Markovian noise for $\omega_0 = 6$ MHz and $2t_c^{-1}$ of 0.05, 0.1, and 0.2 MHz. In all cases, solid curves are fits to analytical expressions for Ramsey decay under non-Markovian noise (Appendix B 2) using the experimental values of ω_0 and $2t_c^{-1}$, with the effective driving strength of the magnetic field as the only free parameter to account for the antenna's impedance.

precession frequency—such as the Larmor frequency of spins in a bath—the observed modulation occurs at the effective frequency $\Omega = \sqrt{\omega_0^2 - t_c^{-2}}$, which deviates from the intrinsic value due to damping. This effect becomes evident only in the strongly damped cases.

The observation of collapses and revivals in the Ramsey signal—predicted by our analytical model for equilibrium underdamped non-Markovian noise—demonstrates that N-V-based sensors can serve as witnesses of non-Markovian dynamics. These nontrivial features reflect how memory and dissipation reshape environmental fluctuations, enabling the sensor to distinguish between noise types and to access both bare and effective parameters. This highlights the relevance of the framework for extracting meaningful statistical information in realistic quantum sensing settings.

We also examined the effect of injected underdamped quenched non-Markovian noise with initial conditions $n(0) = n'(0) = 0$. Figure 4(c) shows Ramsey signals measured upon injection of quenched non-Markovian noise with an effective driving strength A/m^2 of $0.054\ \mathrm{V}^2/\mu\mathrm{s}^3$, a restoring frequency ω_0 of 6 MHz, and damping coefficients $2t_c{}^{-1}$ of 0.05, 0.1, and 0.2 MHz, along with corresponding analytical fits (solid lines). As predicted by the model (Appendixes B 2 and B 4), the collapse and revival features are absent under quenched noise, offering a clear witness of a quench dynamics in underdamped non-Markovian environments. This highlights the importance of careful analysis to ensure that key non-Markovian characteristics are not overlooked.

Moreover, note that all curves corresponding to the quenched cases in Fig. 4(c) overlap. This is because the Ramsey signal remains above the noise floor only for times much shorter than the correlation time t_c, where the leading-order term $(A/40m^2)t^5$ in the attenuation factor dominates. As a result, the attenuation factor is determined solely by the normalized driving strength A/m^2, which is held constant in these experiments.

Overall, these results demonstrate that the Ramsey signal of a N-V center can serve as a sensitive probe of both out-of-equilibrium dynamics—such as quenches—and non-Markovian noise. Crucially, they underscore the importance of accurately resolving the interplay between memory effects and nonstationarity to avoid mischaracterizing the environment in realistic quantum sensing scenarios.

IV. CONCLUSIONS

The use of quantum sensors as witnesses of the statistical nature of noise dynamics offers several advantages. The agreement between the measured Ramsey decay curves and the predictions of our analytical model demonstrates the utility of such models in characterizing noise sources with nonstationary and non-Markovian dynamics—two key features that remain difficult to identify in realistic quantum environments. Having demonstrated that the decay attenuation factor for short evolution times is of higher order for quenched noise, we establish that Ramsey measurements can act as sensitive witnesses of nonstationary noise dynamics. Even when experimental resolution limits the extraction of short-time exponents, complementary signatures at longer times—such as offsets in $\chi(t)$ or the suppression of revivals—provide robust alternative indicators of nonstationary and non-Markovian behavior. This enables us to assess whether a noise source deviates from equilibrium under specific experimental conditions,

either from intrinsic nonstationarity caused by sensor backaction or initialization, or from externally imposed nonstationarity due to driven dynamics. Furthermore, the observation of collapses and revivals in Ramsey decay for stationary underdamped non-Markovian noise highlights the potential of Ramsey measurements to reveal non-Markovian dynamics in noise sources. The results show that the sensor signal encodes not only decoherence rates but also the underlying statistical nature and the nontrivial interplay between nonstationarity and non-Markovianity in the environment. While other dephasing or relaxation channels can obscure the signatures of non-Markovian and nonstationary noise, our experiments demonstrate that the proposed protocol remains viable provided these channels are not significantly stronger than the target environment. In this sense, our framework establishes a baseline scenario that isolates the contribution of environmental noise statistics, offering a clear foundation for interpreting quantum sensing experiments.

The proposed framework not only classifies dynamical noise but also identifies which regimes must be accessed to extract all environmental parameters unambiguously, and how quenching can recover information otherwise inaccessible in stationary measurements. This operational perspective addresses a key challenge in nanoscale noise spectroscopy: full microscopic reconstruction is often impossible, but many practically relevant dynamical features—such as memory, departures from equilibrium, or the presence of few-body dynamics—can be inferred directly from the measured sensor response. Our method therefore complements, rather than replaces, full noise-spectroscopy approaches by providing a lightweight and experimentally accessible route to detect and interpret nonstationarity and non-Markovianity without requiring complete reconstruction of the correlation function.

Characterization of such dynamical features grants insights into the underlying physical mechanisms of the noise—such as hyperpolarization, spin diffusion, or backaction-induced quenches—and also lays the groundwork for developing strategies to mitigate or control these effects. Such strategies may involve optimizing experimental conditions to influence the noise bath or designing pulse sequences tailored to suppress specific noise types, particularly by accounting for memory timescales and deviations from equilibrium [23–30]. These approaches are essential for enhancing the performance and reliability of quantum technologies.

While the present work focuses on Ramsey decay measurements, it opens a pathway to more comprehensive sensing protocols. Future studies could further improve the robustness of noise characterization by incorporating additional pulse sequences, such as a Hahn echo, to reduce parameter dependencies in fitting procedures. Beyond temporal correlations, the characterization of spatial noise correlations presents an exciting direction for future research. Models of spatial correlation functions, such as those proposed for ferromagnetic materials [63], could be experimentally validated by combining spatial and temporal noise measurements. Additionally, while pure dephasing models provide a natural baseline for quantum sensing, an important extension would be to investigate scenarios where the fluctuating field is not aligned with the $\mathrm{N} \rightarrow V$ axis. In such cases, transverse components of the noise could induce relaxation and transitions of the N-V center, expanding the applicability of the present framework to mixed dephasing-relaxation dynamics. This integrated approach would provide deeper insights into noise dynamics, paving the way for improved noise models and better control over quantum systems.

Overall, this work provides a general and experimentally validated method to classify dynamical noise in quantum systems. It enables the detection of (oscillating) non-Markovian and/or nonstationary behavior without fully reconstructing the environmental correlation function. It addresses a key gap in current quantum sensing technology—namely, the lack of frameworks to disentangle and identify the interplay between non-Markovian and nonstationary features— by offering a practical and operationally motivated framework, and paves the way for robust, sensor-based characterization strategies in real-world quantum technologies.

ACKNOWLEDGMENTS

We acknowledge fruitful discussions with Oren Raz on the manuscript, and thank Yoav Romach for his helpful advice on designing the code that controls the Quantum Machines OPX controller (Version 1). A.F. is the incumbent of the Elaine Blond Career Development Chair in Perpetuity and acknowledges funding received from the Minerva Stiftung with the funds from the BMBF of the Federal Republic of Germany and also support from the Kimmel Institute for Magnetic Resonance. This research was made possible in part by the historic generosity of the Harold Perlman Family. G.A.Á. and A.Z. acknowledge support from National Atomic Energy Commission (CNEA); Fundación Balseiro; National Scientific and Technical Research Council (CONICET); Grant No. PIBAA 2022-2023; through National Agency of Scientific and Technological Promotion (ANPCyT)–Fondo para la Investigación Científica y Tecnológica (FONCyT) Grant No. PICT-2018-4333, No. PICT-2021-GRF-TI-00134, and No. PICT-2021-I-A-00070; Proyectos de Investigación Plurianuales (PIP)–CONICET No. 11220170100486CO and No. 11220220100531CO; the Universidad Nacional de Cuyo (UNCUYO) with grants SIIP Tipo I No. 2022-C002, 2022-C030; Instituto Balseiro; the collaboration program between Ministry of Science, Technology and Innovation (MINCyT, Argentina) and the Ministry of Innovation, Science and Technology (MOST, Israel); the

Morris Belkin Visiting Professorship; and the Benoziyo Endowment Fund for the Advancement of Science.

DATA AVAILABILITY

The data that support the findings of this article are openly available [64], embargo periods may apply.

The PYTHON code is available from the authors upon reasonable request.

APPENDIX A: DERIVATION OF CORRELATION FUNCTIONS

1. Markovian noise correlation functions

For the Markovian ($m = 0$) case, $n'(t)$ depends only on the state of the system at the given time t, and the trajectories of the system must satisfy the equation $n' + t_c^{-1} n = (1/\Gamma)\eta(t)$, where $t_c = \Gamma/\kappa$ is the correlation time. The effect of the initial state is described by the homogeneous solutions $n_0(t) = n_0 e^{-\frac{t}{t_c}}$, where the initial state n_0 is independent of the driving—$\langle n_0 \eta(t)\rangle = 0$. To find the trajectory for a particular $\eta(t)$, we can use the Green's function $G(t) = \Theta(t) e^{-\frac{t}{t_c}}$, which has the property $G' + t_c^{-1} G = \delta(t)$. The trajectory is given by $n(t) = n_0(t) + \int_0^t G(t-s)(1/\Gamma)\eta(s) ds$, where the homogeneous part $n_0(t)$ is uniquely determined by the initial condition $n(0) = n_0$. Now recall that the correlation function is defined by the expectation value $\langle n(t_1) n(t_2)\rangle$ for any t_1, t_2 on the same trajectory. Thus, we can treat n_0 as constant when taking the expectation value over a trajectory and afterwards take an average over a distribution of initial conditions to obtain

$$\begin{aligned}\langle n(t_1)\, n(t_2)\rangle &= \left\langle \left(n_0(t_1) + \int_0^{t_1} G(t_1 - s_1)\, \frac{1}{\Gamma} \eta(s_1)\, ds_1 \right) \left(n_0(t_2) + \int_0^{t_2} G(t_2 - s_2)\, \frac{1}{\Gamma} \eta(s_2)\, ds_2 \right) \right\rangle \\ &= \langle n_0(t_1)\, n_0(t_2)\rangle + \int_0^{t_1} \int_0^{t_2} G(t_1 - s_1)\, G(t_2 - s_2)\, \frac{1}{\Gamma^2} \langle \eta(s_1)\, \eta(s_2)\rangle\, ds_2 ds_1. \end{aligned} \tag{A1}$$

Note that this correlation function has two parts: the homogeneous part $\langle n_0(t_1) n_0(t_2)\rangle$, which depends only on the initial condition n_0, and the heterogeneous part, which depends only on the correlation function of the driving force. This general expression can be used for any system for which the Green's function is known. Using the homogeneous solution and Green's function for a Markovian system driven by white noise, we get the homogeneous part $\langle n_0(t_1) n_0(t_2)\rangle = \langle n_0^2\rangle e^{-\frac{t_1+t_2}{t_c}}$ and the heterogeneous part

$$\begin{aligned}\langle n(t_1)\, n(t_2)\rangle - \langle n_0(t_1)\, n_0(t_2)\rangle &= \int_0^{t_1} \int_0^{t_2} e^{-\frac{t_1 - s_1}{t_c}} e^{-\frac{t_2 - s_2}{t_c}} \frac{A}{\Gamma^2} \delta(s_1 - s_2)\, ds_2 ds_1 \\ &= \int_0^{\min(t_1, t_2)} \frac{A}{\Gamma^2} e^{-\frac{t_1 + t_2 - 2s}{t_c}} ds = \frac{A t_c}{2\Gamma^2} \left(e^{-\frac{|t_1 - t_2|}{t_c}} - e^{-\frac{t_1 + t_2}{t_c}} \right), \end{aligned} \tag{A2}$$

so the correlation function for Markovian noise is

$$\langle n(t_1)\, n(t_2)\rangle = \langle n_0^2\rangle e^{-\frac{t_1 + t_2}{t_c}} + \Delta^2 \left(e^{-\frac{|t_1 - t_2|}{t_c}} - e^{-\frac{t_1 + t_2}{t_c}} \right), \tag{A3}$$

where $\Delta^2 = \lim_{t\to\infty} \langle n(t)^2\rangle = A t_c / 2\Gamma^2$ is the variance at equilibrium. At equilibrium, the correlation function is as follows:

$$\lim_{t_1, t_2 \to \infty} \langle n(t_1)\, n(t_2)\rangle = \Delta^2 e^{-\frac{|t_1 - t_2|}{t_c}}. \tag{A4}$$

If we quench the system so that $n_0 = 0$ at the start of each measurement, then the correlation function is as follows:

$$\langle n(t_1)\, n(t_2)\rangle_{n_0 = 0} = \Delta^2 \left(e^{-\frac{|t_1 - t_2|}{t_c}} - e^{-\frac{t_1 + t_2}{t_c}} \right). \tag{A5}$$

Note that if we average $n(t_1) n(t_2)$ over an ensemble with $\langle n_0^2\rangle = \Delta^2$, then the homogeneous part will exactly cancel the transient term in Eq. (A3). If we quench the system at some time t_d before the start of the measurement, then only the nonstationary term will be affected by the delay, so the

correlation function then becomes

$$\langle n\left(t_1\right) n(t_2)\rangle = \Delta^2\left(e^{-\frac{|t_1-t_2|}{t_c}} - e^{-\frac{t_1+t_2+2t_d}{t_c}}\right). \tag{A6}$$

The functional form of this correlation function leads us to the (somewhat surprising) conclusion that a Markovian noise bath is characterized by only two processes: fluctuations with correlation time t_c, and dissipations of (externally imposed) quenches with a decay time of $t_c/2$. The fact that the Fourier transform of the equilibrium term of the Markovian noise correlation function is a Lorentzian explains the ubiquity of Lorentzian noise in nature.

2. Underdamped non-Markovian noise correlation functions

One can use the same method to obtain correlation functions for non-Markovian noise. In particular, we are interested in the $m \neq 0$ case, where the evolution of the noise and its derivative is Markovian, and thus the initial state is described by the initial values (at $t = 0$) of the noise n_0 and of its derivative n_0', and the trajectories of the system satisfy the equation $n'' + 2t_c^{-1}n' + {\omega_0}^2 n = (1/m)\eta(t)$. Depending on the parameters, there are three possible functional forms for the homogeneous solutions $n_0(t)$. When $\omega_0 t_c > 1$, the system is underdamped, and the homogeneous solution is

$$n_0(t) = \left(n_0' + t_c^{-1}n_0\right)\frac{1}{\Omega}\sin\left(\Omega t\right)e^{-\frac{t}{t_c}} + n_0\cos(\Omega t)e^{-\frac{t}{t_c}}, \tag{A7}$$

where $\Omega = \sqrt{{\omega_0}^2 - t_c^{-2}}$. When $\omega_0 t_c < 1$, the system is overdamped, and the homogeneous solution is

$$n_0(t) = \left(n_0' + t_c^{-1}n_0\right)\frac{1}{\alpha}\sinh\left(\alpha t\right)e^{-\frac{t}{t_c}} + n_0\cos(\alpha t)e^{-\frac{t}{t_c}}, \tag{A8}$$

where $\alpha = \sqrt{t_c^{-2} - {\omega_0}^2}$. When $\omega_0 t_c = 1$, the system is critically damped, and the homogeneous solution is

$$n_0(t) = \left(n_0' + t_c^{-1}n_0\right)te^{-\frac{t}{t_c}} + n_0 e^{-\frac{t}{t_c}}. \tag{A9}$$

For the experiments presented in this paper, we restrict ourselves to the underdamped case—which is a typical description of a nuclear spin bath. For the underdamped case, we have the continuous Green's function $G(t) = \Theta(t)(1/\Omega)\sin(\Omega t)e^{-\frac{t}{t_c}}$. Note that, as before, the homogeneous part of the correlation function $\langle n_0(t_1)n_0(t_2)\rangle$ decays to zero for large t_1, t_2, so the equilibrium terms are all contained in the heterogeneous part. For the heterogeneous part, we have

$$\begin{aligned}
\langle n\left(t_1\right) n(t_2)\rangle - \langle n_0\left(t_1\right) n_0(t_2)\rangle &= \int_0^{t_1}\int_0^{t_2}\frac{1}{\Omega^2}\sin\left(\Omega\left(t_1-s_1\right)\right)e^{-\frac{t_1-s_1}{t_c}}\sin\left(\Omega\left(t_2-s_2\right)\right)e^{-\frac{t_2-s_2}{t_c}}\frac{A}{m^2}\delta\left(s_1-s_2\right)ds_2ds_1 \\
&= \frac{A}{2\Omega^2m^2}\int_0^{\min(t_1,t_2)}e^{-\frac{t_1+t_2-2s}{t_c}}\left(\cos\left(\Omega\left(t_1-t_2\right)\right) - \cos\left(\Omega\left(t_1+t_2-2s\right)\right)\right)ds \\
&= \Delta^2\left(\left(\cos\left(\Omega\left(t_1-t_2\right)\right) + \frac{1}{\Omega t_c}\sin\left(\Omega\left|t_1-t_2\right|\right)\right)e^{-\frac{|t_1-t_2|}{t_c}} - \left(\frac{{\omega_0}^2}{\Omega^2}\cos\left(\Omega\left(t_1-t_2\right)\right)\right.\right. \\
&\quad \left.\left. - \frac{1}{\Omega^2t_c^2}\cos\left(\Omega\left(t_1+t_2\right)\right) + \frac{1}{\Omega t_c}\sin\left(\Omega\left(t_1+t_2\right)\right)\right)e^{-\frac{t_1+t_2}{t_c}}\right),
\end{aligned} \tag{A10}$$

where $\Delta^2 = \lim_{t\to\infty}\langle n(t)^2\rangle = At_c/4{\omega_0}^2m^2 = At_c/4m^2(\Omega^2 + t_c^{-2})$ is the variance at equilibrium. Because the transient terms proportional to $e^{-\frac{t_1+t_2}{t_c}}$ disappear in the limit of large t_1, t_2, the correlation function at equilibrium is as follows:

$$\lim_{t_1,t_2\to\infty}\langle n\left(t_1\right) n\left(t_2\right)\rangle = \Delta^2\left(\cos\left(\Omega\left(t_1-t_2\right)\right) + \frac{1}{\Omega t_c}\sin\left(\Omega\left|t_1-t_2\right|\right)\right)e^{-\frac{|t_1-t_2|}{t_c}}. \tag{A11}$$

Also, if we quench the system so that $n_0 = n_0' = 0$, then the homogeneous part will vanish, and the correlation function will consist only of the heterogeneous part. To calculate the equilibrium variance of the derivative $\lim_{t\to\infty}\langle n'(t)^2\rangle$ and the equilibrium covariance $\lim_{t\to\infty}\langle n'(t)n(t)\rangle$, we can use the fact that the correlation function at equilibrium is twice differentiable everywhere (even where $t_1 = t_2$). We then obtain

$$\lim_{t\to\infty}\left\langle n'(t)\,n(t)\right\rangle = \left[\frac{\partial}{\partial t_1}\lim_{t_1,t_2\to\infty}\langle n(t_1)\,n(t_2)\rangle\right]\Bigg|_{t_1=t_2}$$
$$= -\Delta^2\frac{\omega_0^2}{\Omega}\sin(\Omega(t_1-t_2))\,e^{\frac{-|t_1-t_2|}{t_c}}\Bigg|_{t_1=t_2}$$
$$= 0 \tag{A12}$$

and

$$\lim_{t\to\infty}\left\langle n'(t)^2\right\rangle = \left[\frac{\partial^2}{\partial t_2\partial t_1}\lim_{t_1,t_2\to\infty}\langle n(t_1)\,n(t_2)\rangle\right]\Bigg|_{t_1=t_2}$$
$$= \Delta^2\omega_0^2\left(\cos(\Omega(t_1-t_2)) - \frac{1}{\Omega t_c}\sin(\Omega|t_1-t_2|)\right)e^{-\frac{|t_1-t_2|}{t_c}}\Bigg|_{t_1=t_2}$$
$$= \Delta^2{\omega_0}^2. \tag{A13}$$

As before, when we substitute these parameters into the homogeneous part, averaging $n(t_1)n(t_2)$ over some ensemble with $\langle {n_0}^2\rangle = \Delta^2$, $\langle {n_0'}^2\rangle = \Delta^2(\Omega^2 + t_c^{-2}) = \Delta^2{\omega_0}^2$, and $\langle n_0 n_0'\rangle = 0$, the homogeneous part becomes

$$\langle n_0(t_1)n_0(t_2)\rangle = \Delta^2\left(\frac{1}{\Omega t_c}\sin(\Omega(t_1+t_2)) + \frac{{\omega_0}^2}{\Omega^2}\cos(\Omega(t_1-t_2)) - \frac{1}{\Omega^2 t_c^2}\cos(\Omega(t_1+t_2))\right)e^{-\frac{t_1+t_2}{t_c}}, \tag{A14}$$

which exactly cancels the transient terms proportional to $e^{-\frac{t_1+t_2}{t_c}}$ in the heterogeneous part shown in equation (A10), leaving only the equilibrium terms shown in Eq. (A11).

The functional form of $\langle n(t_1)n(t_2)\rangle$ for the noise of an underdamped non-Markovian spin bath shows a much richer behavior than for the Markovian case. One key feature is that the oscillatory behavior of the spin bath persists even at equilibrium. The Fourier transform of the noise from this bath will therefore be centered at the nonzero frequencies $\pm\sqrt{\Omega^2 - t_c^{-2}}$ rather than at zero (see Appendix C).

3. Summary of correlation functions

The correlation functions for equilibrium and quenched Markovian ($m = 0$) noise and underdamped non-Markovian ($m \neq 0$) noise are summarized in Table II.

TABLE II. Correlation functions for equilibrium and quenched ($n_0 = 0$) Markovian noise, and for equilibrium and quenched ($n_0 = n_0' = 0$) underdamped non-Markovian noise.

Noise type	Correlation function $\langle n(t_1)n(t_2)\rangle$
Equilibrium Markovian noise	$\Delta^2 e^{-\frac{\lvert t_1-t_2\rvert}{t_c}}$
Quenched Markovian noise	$\Delta^2\left(e^{-\frac{\lvert t_1-t_2\rvert}{t_c}} - e^{-\frac{t_1+t_2}{t_c}}\right)$
Equilibrium underdamped non-Markovian noise	$\Delta^2\left(\cos(\Omega(t_1-t_2)) + \frac{1}{t_c\Omega}\sin(\Omega\lvert t_1-t_2\rvert)\right)e^{-\frac{\lvert t_1-t_2\rvert}{t_c}}$
Quenched underdamped non-Markovian noise	$\Delta^2\left(\left(\cos(\Omega(t_1-t_2)) + \frac{1}{\Omega t_c}\sin(\Omega\lvert t_1-t_2\rvert)\right)e^{-\frac{\lvert t_1-t_2\rvert}{t_c}} - \left(\frac{{\omega_0}^2}{\Omega^2}\cos(\Omega(t_1-t_2)) - \frac{1}{\Omega^2 t_c^2}\cos(\Omega(t_1+t_2)) + \frac{1}{\Omega t_c}\sin(\Omega(t_1+t_2))\right)e^{-\frac{t_1+t_2}{t_c}}\right)$

APPENDIX B: DERIVATION OF RAMSEY DECAY EXPONENTS

1. Markovian noise Ramsey decay exponents

For equilibrium Markovian noise, the correlation function is written as $\langle n(t_1)n(t_2)\rangle = \Delta^2 e^{\frac{-|t_1-t_2|}{t_c}}$. Thus, the time dependence of the exponent is as follows:

$$\begin{aligned}\chi_{m=0,\mathrm{eq}}(t) &= \int_0^t \int_0^{t_1} \Delta^2 e^{\frac{-|t_1-t_2|}{t_c}} dt_2 dt_1 \\ &= \Delta^2 t_c t - \Delta^2 {t_c}^2 \left(1 - e^{\frac{-t}{t_c}}\right). \end{aligned} \tag{B1}$$

For short times $t \ll t_c$, we can write $\chi_{m=0,\mathrm{eq}}(t) \approx (\Delta^2/2)t^2 - (\Delta^2/6t_c)t^3 + O(t^4)$, and for long times $t \gg t_c$, we can write $\chi_{m=0,\mathrm{eq}}(t) \approx \Delta^2 t_c t - \Delta^2 {t_c}^2 + O(e^{\frac{-t}{t_c}})$.

For quenched Markovian noise, we can write the correlation function as

$$\langle n(t_1)\, n(t_2)\rangle = \Delta^2 \left(e^{\frac{-|t_1-t_2|}{t_c}} - e^{\frac{-t_1+t_2}{t_c}}\right). \tag{B2}$$

Thus, the time dependence of the exponent is as follows:

$$\begin{aligned}\chi_{m=0,\mathrm{qu}}(t) &= \int_0^t \int_0^{t_1} \Delta^2 \left(e^{\frac{-|t_1-t_2|}{t_c}} - e^{\frac{-t_1+t_2}{t_c}}\right) dt_2 dt_1 \\ &= \Delta^2 t_c t - \Delta^2 {t_c}^2 \left(\frac{3}{2} - 2e^{\frac{-t}{t_c}} + \frac{1}{2}e^{\frac{-2t}{t_c}}\right). \end{aligned} \tag{B3}$$

For short times $t \ll t_c$, we can write $\chi_{m=0,\mathrm{qu}}(t) \approx (\Delta^2/3t_c)t^3 + O(t^4) = (A/6\Gamma^2)t^3 + O(t^4)$, and for long times $t \gg t_c$, we can write $\chi_{m=0,\mathrm{qu}}(t) \approx \Delta^2 t_c t - \frac{3}{2}\Delta^2 {t_c}^2 + O(e^{\frac{-t}{t_c}})$. Note how the leading order of the short-time exponent for the quenched Markovian noise is proportional to the (normalized) driving strength A/Γ^2.

For Markovian noise with a quench delay, we can write the correlation function as

$$\langle n(t_1)\, n(t_2)\rangle = \Delta^2 \left(e^{\frac{-|t_1-t_2|}{t_c}} - Qe^{\frac{-t_1+t_2}{t_c}}\right), \tag{B4}$$

with $Q = e^{\frac{-2t_d}{t_c}}$. Thus, the linearity of the double integral gives us the time dependence of the exponential as

$$\chi_{m=0,\mathrm{del}}(t; t_d) = (1-Q)\,\chi_{m=0,\mathrm{eq}}(t) + Q\chi_{m=0,\mathrm{qu}}(t). \tag{B5}$$

This indicates that one can use the Ramsey signal to determine the time of a quench relative to the start of the Ramsey experiment.

For Markovian noise with a switch in correlation time, where the correlation time abruptly switches from t_a to t_b at some time t_s, we can write the correlation function as

$$\langle n(t_1)\, n(t_2)\rangle = \begin{cases} \Delta^2 e^{\frac{-|t_1-t_2|}{t_a}} & \text{for } t_1, t_2 \le t_s, \\ \Delta^2 e^{\frac{-t_s-t_1}{t_a} - \frac{t_2-t_s}{t_b}} & \text{for } t_1 < t_s < t_2, \\ \Delta^2 e^{\frac{-t_s-t_2}{t_a} - \frac{t_1-t_s}{t_b}} & \text{for } t_2 < t_s < t_1, \\ \Delta^2 e^{\frac{-|t_1-t_2|}{t_b}} & \text{for } t_1, t_2 \ge t_s. \end{cases} \tag{B6}$$

Thus, the time dependence of the exponent will also change abruptly at t_s. For $t \le t_s$, we have

$$\begin{aligned}\chi_{m=0,\mathrm{sw},t\le t_s}(t) &= \int_0^t \int_0^{t_1} \Delta^2 e^{\frac{-|t_1-t_2|}{t_a}} dt_2 dt_1 \\ &= \Delta^2 t_a t - \Delta^2 {t_a}^2 \left(1 - e^{\frac{-t}{t_a}}\right). \end{aligned} \tag{B7}$$

For $t > t_s$, we have to split the double integral into three regions, and we have

$$\begin{aligned}\chi_{m=0,\mathrm{sw},t>t_s}(t) &= \int_0^{t_s} \int_0^{t_1} \Delta^2 e^{\frac{-|t_1-t_2|}{t_a}} dt_2 dt_1 + \int_{t_s}^t \int_{t_s}^{t_1} \Delta^2 e^{\frac{-|t_1-t_2|}{t_a}} dt_2 dt_1 + \int_{t_s}^t \int_0^{t_s} \Delta^2 e^{\frac{-t_s-t_2}{t_a} - \frac{t_1-t_s}{t_b}} dt_2 dt_1 \\ &= \Delta^2 t_a t_s - \Delta^2 {t_a}^2 \left(1 - e^{\frac{-t_s}{t_a}}\right) + \Delta^2 t_b (t - t_s) - \Delta^2 {t_b}^2 \left(1 - e^{\frac{-t-t_s}{t_b}}\right) + \Delta^2 t_a t_b \left(1 - e^{\frac{-t_s}{t_a}}\right)\left(1 - e^{\frac{-t-t_s}{t_b}}\right). \end{aligned} \tag{B8}$$

This indicates that one can use the Ramsey signal to determine the time of an abrupt change in the correlation time, provided one acquires enough time points before and after the switch.

2. Underdamped non-Markovian Ramsey decay exponents

For equilibrium underdamped non-Markovian ($m \neq 0$) noise, the correlation function is as follows:

$$\langle n(t_1)\, n(t_2)\rangle = \Delta^2 \left(\cos(\Omega(t_1 - t_2)) + \frac{1}{\Omega t_c}\sin(\Omega|t_1 - t_2|)\right) e^{-\frac{|t_1-t_2|}{t_c}}, \tag{B9}$$

where $\Omega = \sqrt{\omega_0{}^2 - t_c^{-2}}$ is the damped frequency of the oscillator. Thus, the time dependence of the exponent is as follows:

$$\begin{aligned}\chi_{m\neq 0,\mathrm{eq}}(t) &= \int_0^t \int_0^{t_1} \Delta^2 \left(\cos(\Omega(t_1 - t_2)) + \frac{1}{\Omega t_c}\sin(\Omega|t_1 - t_2|)\right) e^{-\frac{|t_1 - t_2|}{t_c}} dt_2 dt_1 \\ &= \frac{2\Delta^2}{t_c \omega_0{}^2} t - \frac{\Delta^2}{\omega_0{}^4}\left(\left(\Omega^2 - 3t_c^{-2}\right)\cos(\Omega t) + \frac{\left(3\Omega^2 - t_c^{-2}\right)}{\Omega t_c}\sin(\Omega t)\right) e^{-\frac{t}{t_c}} + \frac{\Delta^2\left(\Omega^2 - 3t_c^{-2}\right)}{\omega_0{}^4}. \end{aligned} \tag{B10}$$

For short times $t \ll t_c, 1/\Omega$, we can write $\chi_{m\neq 0,\mathrm{eq}}(t) \approx (\Delta^2/2)t^2 - (\Delta^2\omega_0{}^2/24)t^4 + (\Delta^2\omega_0{}^2/60t_c)t^5 + O(t^6)$, and for long times $t \gg t_c, 1/\Omega$, we can write $\chi_{m\neq 0,\mathrm{eq}}(t) \approx (2\Delta^2/t_c\omega_0{}^2)t + \Delta^2(\Omega^2 - 3t_c^{-2})/\omega_0{}^4 + O(e^{-\frac{t}{t_c}})$.

For quenched underdamped non-Markovian noise (when $n_0 = n_0' = 0$), the correlation function differs from the equilibrium correlation function by a transient term:

$$\begin{aligned}\langle n(t_1)\, n(t_2)\rangle_{\mathrm{tr}} &= \langle n(t_1)\, n(t_2)\rangle - \langle n(t_1)\, n(t_2)\rangle_{\mathrm{eq}} \\ &= -\Delta^2\left(\frac{\omega_0{}^2}{\Omega^2}\cos(\Omega(t_1 - t_2)) - \frac{1}{\Omega^2 t_c^2}\cos(\Omega(t_1 + t_2)) + \frac{1}{\Omega t_c}\sin(\Omega(t_1 + t_2))\right) e^{-\frac{t_1 + t_2}{t_c}}. \end{aligned} \tag{B11}$$

This transient term changes the time dependence of the exponent by

$$\begin{aligned}\chi_{m\neq 0,\mathrm{tr}}(t) &= -\Delta^2 \int_0^t \int_0^{t_1} e^{-\frac{t_1 + t_2}{t_c}}\left(\frac{\omega_0{}^2}{\Omega^2}\cos(\Omega(t_1 - t_2)) - \frac{1}{\Omega^2 t_c^2}\cos(\Omega(t_1 + t_2)) + \frac{1}{\Omega t_c}\sin(\Omega(t_1 + t_2))\right) dt_2 dt_1 \\ &= -\frac{\Delta^2}{\omega_0{}^4}\left[\left(\frac{\omega_0{}^4}{2\Omega^2} + \frac{\left(3\Omega^2 - t_c^{-2}\right)}{2\Omega^2 t_c^2}\cos(2\Omega t) + \frac{\left(3t_c^{-2} - \Omega^2\right)}{2\Omega t_c}\sin(2\Omega t)\right) e^{-\frac{2t}{t_c}}\right. \\ &\quad \left. + \left(-\left(\Omega^2 + 5t_c^{-2}\right)\cos(\Omega t) + \frac{\left(\Omega^2 - 3t_c^{-2}\right)}{\Omega t_c}\sin(\Omega t)\right) e^{-\frac{t}{t_c}} - \left(\frac{\omega_0{}^4}{2\Omega^2} + \frac{\left(3\Omega^2 - t_c^{-2}\right)}{2\Omega^2 t_c^2} - \left(\Omega^2 + 5t_c^{-2}\right)\right)\right]. \end{aligned} \tag{B12}$$

For short times $t \ll t_c, \Omega^{-1}$, we can write $\chi_{N=2,\mathrm{tr}}(t) \approx -(\Delta^2/2)t^2 + (\Delta^2\omega_0{}^2/24)t^4 + (\Delta^2\omega_0{}^2/12t_c)t^5 + O(t^6)$, so we have $\chi_{m\neq 0,\mathrm{qu}}(t) = \chi_{m\neq 0,\mathrm{eq}}(t) + \chi_{m\neq 0,\mathrm{tr}}(t) \approx (\Delta^2\omega_0{}^2/10t_c)t^5 + O(t^6) = (A/40m^2)t^5 + O(t^6)$, and for long times $t \gg t_c, \Omega^{-1}$, we can write $\chi_{m\neq 0,\mathrm{tr}}(t) \approx (\Delta^2/\omega_0{}^4)(\omega_0{}^4/2\Omega^2) + (3\Omega^2 - t_c^{-2})/2\Omega^2 t_c^2 - (\Omega^2 + 5t_c^{-2})) + O(e^{-\frac{t}{t_c}})$, so we have $\chi_{m\neq 0,\mathrm{qu}}(t) = \chi_{m\neq 0,\mathrm{eq}}(t) + \chi_{m\neq 0,\mathrm{tr}}(t) \approx (2\Delta^2/t_c\omega_0{}^2)t + \Delta^2/2\Omega^2 + \Delta^2(3\Omega^2 - t_c^{-2})/2\Omega^2 t_c^2\omega_0{}^4 - 8\Delta^2/t_c^2\omega_0{}^4 + O(e^{-\frac{t}{t_c}})$. Note how the leading order of the short-time exponent for the quenched non-Markovian noise is proportional to the (normalized) driving strength A/m^2.

3. Summary of Ramsey decay exponents

The short-time and long-time approximations of the Ramsey decay exponents for equilibrium and quenched Markovian ($m = 0$) noise and underdamped non-Markovian ($m \neq 0$) noise are summarized in the Table III:

4. Analytical plots of Ramsey decay curves for non-Markovian noise

Plots of predicted Ramsey decay curves for quenched and equilibrium underdamped non-Markovian noise are shown in Fig. 5. Note that, as discussed in the main text, the peak of the revival in the Ramsey decay curve for equilibrium underdamped non-Markovian noise always coincides with a minimum in the absolute value of the derivative of the Ramsey decay curve for quenched underdamped non-Markovian noise. When the quantum sensor is subject only to quenched underdamped non-Markovian noise, these plateaus at $t = 2\pi m/\Omega$ for $m \in \mathbb{Z}^*$ are readily apparent. However, in our experiment, in addition to injected noise, there is also native noise from the diamond itself (see Fig. 7), which gives rise to a finite T_2^* decay time even in the absence of injected noise. When the effect of this T_2^* is included, the inflection points in the Ramsey decay curve for quenched underdamped non-Markovian noise become less apparent, as one can see by comparing the red and blue curves in Fig. 5.

TABLE III. Short-time and long-time approximations of the Ramsey decay exponents $\chi(t)$ for the noise types described in Table II. The Ramsey decay is given by $\langle S_z \rangle = e^{-\chi(t)}$.

Noise type	Ramsey exponent $\chi(t)$, short time	Ramsey exponent $\chi(t)$, long time
Equilibrium Markovian noise	$\chi(t) \approx \frac{\Delta^2}{2}t^2 - \frac{\Delta^2}{6t_c}t^3 + O(t^4)$	$\chi(t) \approx \Delta^2 t_c t - \Delta^2 {t_c}^2 + O(e^{\frac{-t}{t_c}})$
Quenched Markovian noise	$\chi(t) \approx \frac{\Delta^2}{3t_c}t^3 + O(t^4) = \frac{1}{6}\frac{A}{\Gamma^2}t^3 + O(t^4)$	$\chi(t) \approx \Delta^2 t_c t - \frac{3}{2}\Delta^2 {t_c}^2 + O(e^{\frac{-t}{t_c}})$
Equilibrium underdamped non-Markovian noise	$\chi(t) \approx \frac{\Delta^2}{2}t^2 - \frac{\Delta^2 {\omega_0}^2}{24}t^4 + \frac{\Delta^2 {\omega_0}^2}{60t_c}t^5 + O(t^6)$	$\chi(t) \approx \frac{\Delta^2}{t_c\left(\Omega^2 + t_c^{-2}\right)^2}t + \Delta^2\frac{\Omega^2 - 3t_c^{-2}}{\left(\Omega^2 + t_c^{-2}\right)^2} + O\left(e^{-\frac{t}{t_c}}\right)$
Quenched underdamped non-Markovian noise	$\chi(t) \approx \frac{\Delta^2 {\omega_0}^2}{10t_c}t^5 + O(t^6) = \frac{A}{40m^2}t^5 + O(t^6)$,	$\chi(t) \approx \frac{2\Delta^2}{t_c {\omega_0}^2}t + \frac{\Delta^2}{2\Omega^2} + \frac{\Delta^2\left(3\Omega^2 - t_c^{-2}\right)}{2\Omega^2 t_c^2 {\omega_0}^4} - \frac{8\Delta^2}{t_c^2 {\omega_0}^4} + O\left(e^{-\frac{t}{t_c}}\right)$

5. A note on the parameters of $\chi(t)$ shown above

Note that for the Markovian ($m = 0$) case, we keep the equilibrium variance $\Delta^2_{m=0}$ constant and vary the correlation time t_c, so the equilibrium Ramsey decay remains constant and the quenched Ramsey decay becomes slower as t_c increases (see Fig. 2), as predicted by the expressions for $\chi(t)$ in Appendix B 1. For the non-Markovian ($m \neq 0$) case, we keep the driving strength A/m^2 constant and vary the self-correlation time t_c. Therefore, as t_c increases, the equilibrium variance for the non-Markovian case $\Delta^2_{m\neq 0} = At_c/4{\omega_0}^2 m^2$ increases, so the equilibrium Ramsey decay becomes faster and the quenched Ramsey decay remains constant (see Fig. 4), as predicted by the expressions for $\chi(t)$ in Appendix B 2.

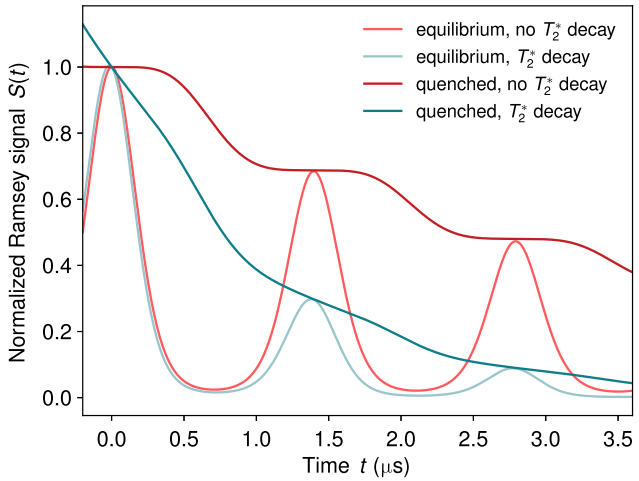

FIG. 5. Analytical calculation of the Ramsey signal for equilibrium (light red, light blue) and quenched (red, blue) underdamped non-Markovian ($m \neq 0$) injected noise with a driving strength A/m^2 of 400 $M\text{Hz}^5$, restoring frequency of 5 MHz, and damping coefficient of 0.2 MHz both without (red) and with (blue) an independent T_2^* of 1.67 μs from noninjected white noise.

APPENDIX C: EQUILIBRIUM NOISE SPECTRAL DENSITIES FOR MARKOVIAN AND UNDERDAMPED NOISE

Using the fact that the correlation functions for equilibrium noise are invariant to translations in time, we can define the equilibrium noise spectral density,

$$S(\omega) = \frac{1}{2\pi}\int_{-\infty}^{\infty}\langle n(t)n(0)\rangle e^{i\omega t}dt. \tag{C1}$$

For equilibrium Markovian noise, the noise spectral density is expressed as

$$S_{m=0}(\omega) = \frac{\Delta^2}{2\pi}\int_{-\infty}^{\infty}e^{-|t|/t_c + i\omega t}dt = \frac{\Delta^2}{\pi}\frac{t_c}{1 + t_c^2\omega^2}, \tag{C2}$$

which peaks at $\omega = 0$ and decays as $O(\omega^2)$ for large ω. The fact that the noise spectrum of a Markovian noise process is Lorentzian explains the ubiquity of Lorentzian noise spectra in nature. For equilibrium underdamped non-Markovian noise, the noise spectral density is expressed as

$$\begin{aligned} &S_{m\neq 0}(\omega) \\ &= \frac{\Delta^2}{2\pi}\int_{-\infty}^{\infty}\left(\cos(\Omega t) + \frac{1}{t_c\Omega}\sin(|\Omega t|)\right)e^{-|t|/t_c + i\omega t}dt \\ &= \frac{2\Delta^2{\omega_0}^2}{\pi t_c}\frac{1}{\left(\omega^2 - \omega_0^2\right)^2 + 4t_c^{-2}\omega^2}, \end{aligned} \tag{C3}$$

which peaks at $\omega = \pm\sqrt{\omega_0^2 - 2t_c^{-2}}$ (or at 0 if $\omega_0 t_c < \sqrt{2}$) and decays as $O(\omega^4)$ for large ω. The lower spectral density for large ω results from the fact that the first derivative

of a non-Markovian noise trajectory must be continuous. Indeed, simply by comparing the trajectories in Figs. 1(b) and 1(c), one can observe that the discontinuities in the first derivative of the Markovian noise trajectories give rise to stronger higher-frequency components.

APPENDIX D: PHYSICAL REALIZATIONS OF THE $m \neq 0$ MODEL

In this appendix we show physical realizations of the $m \neq 0$ model. This shows how different physical cases, including quantum systems, can give rise to noise closely resembling that of classical stochastic processes.

1. Damped quantum harmonic oscillator

A possible application of the $m \neq 0$ model is a quantum sensor coupled to the position of a quantum harmonic oscillator dampened due to interacting with a finite-temperature Caldeira-Legget bath with Ohmic spectral density. The evolution of the position $n(t)$ of this system is described by [65]

$$n''(t) + 2t_c^{-1}n'(t) + \omega_0^2 n(t) = \frac{F(t)}{m}, \tag{D1}$$

where $F(t)$ is the fluctuating force felt by the oscillator due to its environment. $F(t)$ need not be white; however, under certain conditions, such as high temperature, white noise can be recovered from this system. Moreover, when the harmonic oscillator is underdamped (i.e., weakly coupled to the Caldeira-Legget bath), its dynamics will act as a bandpass filter where the system can exchange energy only with the modes of frequency ω_0. In this case, the correlation function of $F(t)$ becomes irrelevant, as only the value of its noise spectrum at ω_0 will affect the oscillator dynamics. To see an example of this, consider the stationary noise spectrum of the oscillator [65]

$$S(\omega) = \frac{2}{mt_c}\frac{\omega \coth\left(\frac{\omega}{2T}\right)}{\left(\omega^2 - \omega_0^2\right)^2 + 4t_c^{-2}\omega^2}, \tag{D2}$$

where T is the temperature and $\hbar = k_B = 1$. Note that this noise spectrum does not match that of a classical $m \neq 0$ process, as the term $\omega\coth(\omega/2T)$ induces an extra dependence on the frequency. However, at high temperature, we can take $\omega\coth(\omega/2T) \approx 2T$ and obtain

$$S(\omega) = \frac{4T}{t_c m}\frac{1}{\left(\omega^2 - \omega_0^2\right)^2 + 4t_c^{-2}\omega^2}, \tag{D3}$$

which does match our model. But it is not necessary to take the high-temperature limit, as if $\omega t_c \gg 1$, the noise spectrum will be composed of two peaks, at $\omega = \pm\sqrt{\omega_0^2 - 2t_c^{-2}}$, in the same positions as the peaks of $S_{m\neq 0}(\omega)$ in Appendix C. Thus, when studying the peaks of the spectrum, we can write the approximation

$$S(\omega) = \frac{2}{t_c m}\omega_0 \coth\left(\frac{\omega_0}{2T}\right)\frac{1}{\left(\omega^2 - \omega_0^2\right)^2 + 4t_c^{-2}\omega^2}, \tag{D4}$$

which again matches the results of our model. As seen in Eq. (D1), the parameter m of our model coincides with the physical mass of the harmonic oscillator in this case.

2. Rotating spin bath

We consider the case where the N-V center couples to a bath of environmental spins that, in addition to experiencing thermal fluctuations, also precess with frequency Ω. To model this class of systems in the simplest possible terms, we consider that the environmental operator that induces dephasing in the N-V center is $n \propto I_x$, where

$$\mathbf{I} = \begin{pmatrix} I_x \\ I_y \end{pmatrix} \tag{D5}$$

is the environmental magnetization, restricted to the direction perpendicular to Larmor precession. When the N-V center interacts with many environmental spins, the environmental field $\mathbf{I}$ may be replaced by a Gaussian, semiclassical random process. We describe this process with the stochastic differential equation

$$\mathbf{I}'(t) = \begin{pmatrix} -t_c^{-1} & \Omega \\ -\Omega & -t_c^{-1} \end{pmatrix}\mathbf{I}(t) + \boldsymbol{\eta}, \tag{D6}$$

where Ω is the effective rotation frequency of the bath spins, t_c^{-1} is the lifetime of their magnetization, and $\boldsymbol{\eta}$ is a two-dimensional meanless Gaussian white noise process. Its correlation function is $\langle \boldsymbol{\eta}(t_1) \otimes \boldsymbol{\eta}(t_2)\rangle = A\delta(t_2 - t_1)\mathbb{I}_2$, where $\mathbb{I}_2$ is the 2×2 identity matrix.

To solve this equation, as before, use again Green's functions, and write

$$\mathbf{I}(t) = \mathbf{I}_0(t) + \int_0^t \mathbb{G}(t-s)\boldsymbol{\eta}(s)ds, \tag{D7}$$

where

$$\mathbf{I}_0(t) = e^{-\frac{t}{t_c}}\begin{pmatrix} \cos(\Omega t) & \sin(\Omega t) \\ -\sin(\Omega t) & \cos(\Omega t) \end{pmatrix}\mathbf{I}_0 \tag{D8}$$

is the homogeneous solution describing the decay of initial conditions and $\mathbb{G}$ is the Green's function, which satisfies

$$\mathbb{G}'(t) - \begin{pmatrix} -t_c^{-1} & \Omega \\ -\Omega & -t_c^{-1} \end{pmatrix}\mathbb{G}(t) = \delta(t)\mathbb{I}_2. \tag{D9}$$

It is given by

$$\mathbb{G}(t) = \Theta(t)e^{-\frac{t}{t_c}}\begin{pmatrix} \cos(\Omega t) & \sin(\Omega t) \\ -\sin(\Omega t) & \cos(\Omega t) \end{pmatrix}. \tag{D10}$$

After performing the same procedure as in Appendix A, we obtain the correlation function for the noise process $n(t)$ as

$$\langle n(t_1)n(t_2)\rangle = \Delta^2 e^{-\frac{|t_2-t_1|}{t_c}}\cos\left(\Omega\left(t_2-t_1\right)\right) + e^{-\frac{t_1+t_2}{t_c}}\left[\left(\frac{\langle \mathbf{I}_0^2\rangle}{2}-\Delta^2\right)\cos\left(\Omega\left(t_1-t_2\right)\right)+\frac{\langle I_{0x}^2\rangle-\langle I_{0y}^2\rangle}{2}\cos\left(\Omega\left(t_1+t_2\right)\right)+\langle I_{0x}I_{0y}\rangle\sin\left(\Omega\left(t_1+t_2\right)\right)\right], \tag{D11}$$

where Δ^2 is the equilibrium variance of $n(t)$. The homogeneous and heterogeneous parts are, respectively,

$$\langle n_0(t_1)n_0(t_2)\rangle = e^{-\frac{t_1+t_2}{t_c}} \times\left[\frac{\langle \mathbf{I}_0^2\rangle}{2}\cos\left(\Omega\left(t_1-t_2\right)\right)+\frac{\langle I_{0x}^2\rangle-\langle I_{0y}^2\rangle}{2}\cos\left(\Omega\left(t_1+t_2\right)\right)+\langle I_{0x}I_{0y}\rangle\sin\left(\Omega\left(t_1+t_2\right)\right)\right], \tag{D12a}$$

$$\langle n(t_1)n(t_2)\rangle - \langle n_0(t_1)n_0(t_2)\rangle = \Delta^2\left(e^{-\frac{|t_2-t_1|}{t_c}}-e^{\frac{t_1+t_2}{t_c}}\right)\cos\left(\Omega\left(t_2-t_1\right)\right). \tag{D12b}$$

Note the resemblance to Eqs. (A7) and (A10). In particular, in the very underdamped limit, $\Omega t_c \to \infty$, the two expressions match, showing that our $m \neq 0$ model recovers the behavior of this spin-bath model in the limit where the spins precess many times before decaying. However, since the correlation function is not smooth (as it has a cusp at $t_1 = t_2$), the noise spectrum will be $O(\omega^2)$ and not $O(\omega^4)$. However, the oscillatory behavior in the self-correlation function will induce the same type of revivals in the Ramsey experiments as in the $m \neq 0$ process.

3. Asymmetric spin bath

We also consider a more general process for modeling the environmental spins, where we replace Eq. (D6) by

$$\mathbf{I}'(t) = \begin{pmatrix} -t_{cx}^{-1} & \omega_0 \\ -\omega_0 & -t_{cy}^{-1}\end{pmatrix}\mathbf{I}(t) + \Sigma\boldsymbol{\eta}, \tag{D13}$$

where t_{cx} and t_{cy} are the decay times in the x and y axes of the spin I, ω_0 is the bare Larmor frequency, and

$$\Sigma = \begin{pmatrix} \sigma_x & \sigma_{xy} \\ \sigma_{xy} & \sigma_y\end{pmatrix} \tag{D14}$$

is a 2×2 constant matrix that couples the white noise process $\boldsymbol{\eta}$ to the semiclassical process $\mathbf{I}$. This model includes anisotropy in the magnetization decay, as well as in the fluctuations. We focus on the limit where $t_{cx}^{-1}, \sigma_x, \sigma_{xy} \to 0$, and take $t_{cy} = t_c/2$, $\sigma_y = (m\omega_0)^{-1}$, and $\eta = \eta_y$. In this case, Eq. (D13) simplifies to

$$\mathbf{I}'(t) = \begin{pmatrix} 0 & \omega_0 \\ -\omega_0 & -2t_c^{-1}\end{pmatrix}\mathbf{I}(t) + \begin{pmatrix} 0 \\ \frac{\eta(t)}{m\omega_0}\end{pmatrix}. \tag{D15}$$

If we note that taking the inner product of both sides of equation (D15) with $\hat{\mathbf{x}} = \begin{pmatrix}1\\0\end{pmatrix}$ gives $I_x'(t) = \omega_0 I_y(t)$, after taking $n(t) = I_x(t)$ and $n'(t) = \omega_0 I_y(t)$, we obtain

$$n''(t) + 2t_c^{-1}n' + \omega_0^2 n(t) = \eta(t)/m, \tag{D16}$$

which coincides with Eq. (3). Since same the stochastic differential equation describes both processes, the correlation functions of the processes are the same. In this case, the parameter $m = (\omega_0\sigma_y)^{-1}$ represents not a physical mass but an effective quantity encapsulating the Larmor frequency and the strength of coupling to other environmental degrees of freedom, modeled as an external white-noise process.

This is a spin model where the N-V center is coupled to a direction where the environment fluctuation and relaxation dynamics is suppressed, but that is mixed through Larmor precession with an axis to which the N-V center does not couple directly, but that experiences relaxation and fluctuations. We have shown thus that this spin model behaves exactly as the $m \neq 0$ model we presented in the main text.

APPENDIX E: EXPERIMENTAL METHODS

1. N-V center experimental setup

The N-V centers used for our experiments are on nanopillar arrays [66] on a diamond membrane. The membrane is mounted on a movable stage above a confocal microscope, which focuses a 520 nm green laser on the sample to excite the N-V center. The position of the focal point can be controlled with nanometer resolution with the use of galvanometer mirrors. The broad red-infrared fluorescence (red of the zero-phonon line at 637 nm) is

redirected to two single-photon counters by means of a dichroic mirror and a beam splitter. The photon counts are then read by a time tagger and an avalanche photodiode with a resolution of 300 ps.

2. Spin state control of the N-V center

The direction of the static magnetic field is controlled by manipulation of the position of a permanent magnet above the diamond. To ensure a high fluorescence contrast, the direction of this field is chosen to align with the axis of symmetry of the N-V center, determined by maximization of the difference in the frequencies of the $|0\rangle \leftrightarrow |1\rangle$ and $|0\rangle \leftrightarrow |-1\rangle$ transitions, which is evaluated by ODMR measurements.

The spin state of the N-V center is manipulated by application of MW pulses created by mixing a MW signal with a signal from an arbitrary waveform generator. These pulses are then passed to a copper wire running above the surface of the diamond. All experiments are managed with QUDI [67], PYTHON-based software designed for performing quantum sensing measurements using N-V centers.

3. Characterization and control measurements on the N-V center

To see the effect of injected noise, one must first find a N-V center whose local noise environment has a sufficiently low amplitude, so that one can distinguish the effect of injected noise from the effect of environmental noise. After examining several N-V defects, we found a suitable N-V center, which is marked by a dotted white rectangle in the fluorescence microscope image in Fig. 6(a). To characterize this N-V center, we performed ODMR and Rabi measurements, as shown in Figs. 6(b) and 6(c). These measurements were done after we had aligned the magnetic field with the N-V axis by finding the magnet position that maximizes the ODMR splitting. On the basis of the shift of the $|0\rangle \leftrightarrow |-1\rangle$ peak from the zero-field splitting of 2.87 GHz, we calculate the applied static magnetic field to be 298 G. The Rabi measurement shows this N-V center has a Rabi contrast of 34.1% and a π time of 344 ns.

Following this, we conducted two control experiments. To determine the effective T_2^* of the N-V center, we performed a (drift-corrected) Ramsey measurement with no injected noise, as shown in Fig. 7(a). Assuming white noise from the environment, the T_2^* fitted from this measurement is 1.65 μs. To estimate the coupling between the N-V center and the spiral, we also performed a Ramsey measurement, where a constant potential of 0.45 V was applied to the spiral (the maximum potential we can apply is 0.5 V). The Ramsey signal from this experiment, shown in Fig. 7(b), shows an oscillation at 3.6 MHz, which is significantly faster than the decay rate of 0.608 μs^{-1}, indicating that this N-V center is suitable for our injected noise measurements.

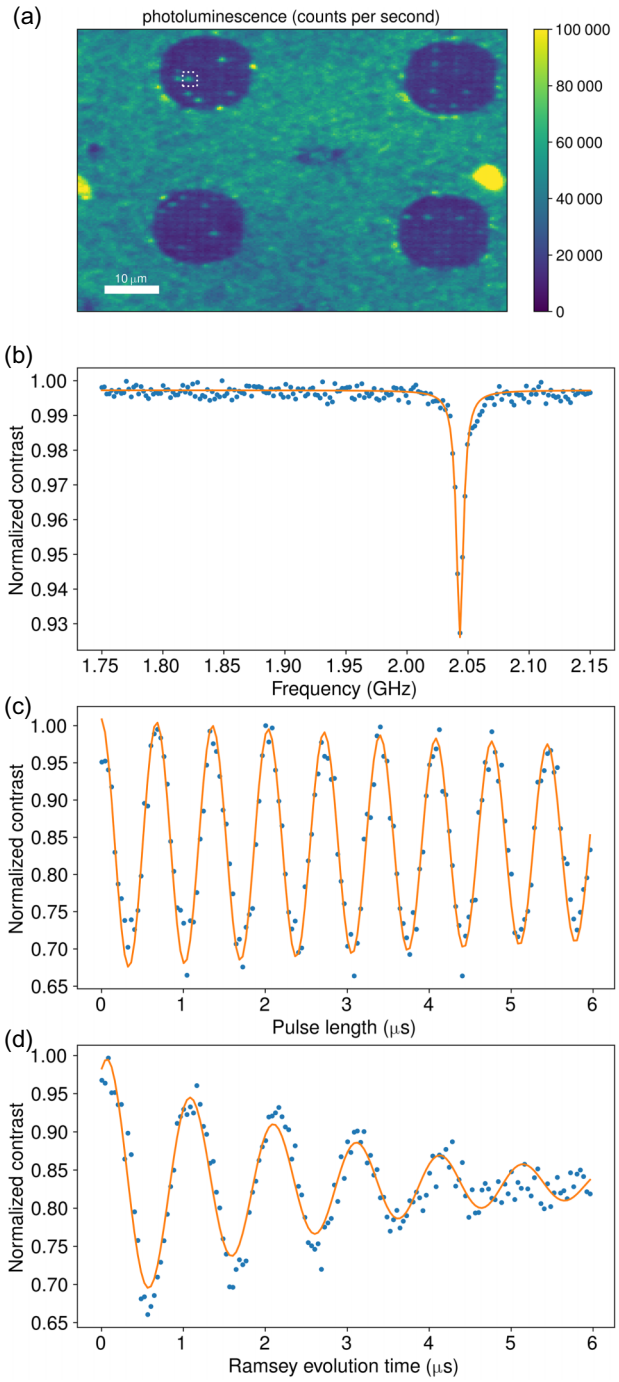

FIG. 6. (a) Confocal fluorescence microscope image showing the diamond used for the measurements presented in the main text. The dotted array consists of nanopillars fabricated to increase photon collection efficiency [66]. Some of them are bright and host a single N-V center. The one used here is marked by a dotted white square. (b) ODMR spectrum in the 1.75–2.15 GHz range, showing the $|0\rangle \leftrightarrow |-1\rangle$ transition used for the measurements presented in (c),(d). (c) Rabi measurement at the $|0\rangle \leftrightarrow |-1\rangle$ transition, showing a contrast of 34.1% and a π time of 344 ns. (d) Ramsey measurement with a detuning of 1 MHz, showing a T_2^* time of 3.52 μs.

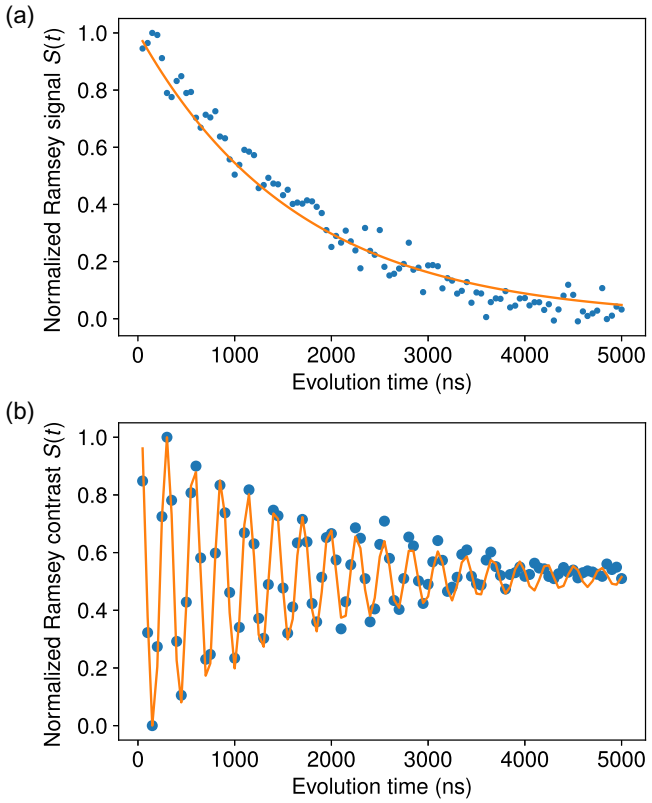

FIG. 7. Control measurements for the N-V center. (a) Drift-corrected Ramsey signal, showing the T_2^* time without a detuning. (b) Ramsey signal with an injection of constant 0.45 V signal, giving rise to a 3.6 MHz oscillation.

4. Injection of noise and Ramsey decay measurements

A realization of the desired type of noise is sent as an updated waveform to a Quantum Machines OPX controller, and the analog channel outputs the noise during the evolution time of the Ramsey sequence. A description of the noise generation algorithms for each noise type is given in Appendix E 5.

The noise is passed to a spiral antenna [68] below the diamond, with a hole in the center of the spiral to allow the green laser to excite any N-V center in the exposed region of the diamond. Since we are using a spiral on the surface of the diamond to inject our noise, the magnetic field created by this current, measured in the center of the spiral, will always be perpendicular to the surface of the diamond, at some fixed angle with the z axis of the N-V center. Therefore, all of the N-V centers in this region experience a magnetic field proportional to the amplitude of the voltage supplied from the analog channel of the Quantum Machines OPX controller.

To measure the effect of each type of injected noise on the Ramsey trace of our N-V center, it is necessary, for each delay time, both to perform enough repetitions to appropriately measure the expectation value $\langle S_z \rangle$ after the Ramsey sequence and to inject enough realizations of the noise so that $\langle S_z \rangle$ at each delay time will be sensitive to the full distribution of noise realizations.

To implement this, we conduct the measurement of each Ramsey trace using four nested loops. The innermost loop carries out 4×10^5 Ramsey measurements for each realization at a given evolution time, the second loop carries out the first loop for ten different realizations of noise for each evolution time, the third loop carries out the second loop for 100 different values of the evolution time, from 25 to 2500 ns, and the fourth loop carries out the third loop ten times, for a total of 100 realizations per time point. The fourth loop is necessary so that any unexpected changes to the system will affect all time points.

Additionally, to minimize the effect of drift in the static magnetic field, every 30 min, the measurement cycle is paused, and a regular Ramsey measurement is performed with no injected noise, but with a 1 MHz offset in the MW frequency. The PYTHON program uses the results of this measurement to adjust the MW frequency to correct for this drift, and then measures another regular Ramsey measurement with a 1 MHz offset to ensure that the correction was successful before continuing with the injected-noise Ramsey measurements.

We note that, in principle, factors such as crosstalk, impedance mismatches, or antenna geometry could distort the injected noise. In our implementation, however, no systematic deviations attributable to these effects were observed: the measured Ramsey signals were accurately described by the analytical predictions across all regimes, including underdamped non-Markovian noise, where such distortions would be most apparent. If required, these effects could be further mitigated by characterization of the antenna transfer function and compensation for the injected-noise spectrum accordingly.

5. Algorithms for generation of each noise type

To implement the experiments, we generated discrete-time realizations of stochastic processes designed to reproduce the analytical correlation functions derived in Appendix A. In this section we describe the algorithms used to produce each type of injected noise.

a. Generation of Markovian noise trajectories

Because the correlation function for equilibrium Markovian noise has only one term, it is simple to generate this type of noise directly. As shown in Appendix A 1, Markovian noise has a correlation time given by t_c, and at equilibrium, the variance at each time point is constant $\langle n(t)^2 \rangle = \Delta^2$. To produce Markovian noise at a series of time points $0, \Delta t, 2\Delta t, \ldots, t_{\text{total}} - \Delta t$, we sample the first point from $N(0, \Delta_M)$—the normal distribution with mean 0 and standard deviation Δ_M. For each subsequent point, we either retain the value of the previous point

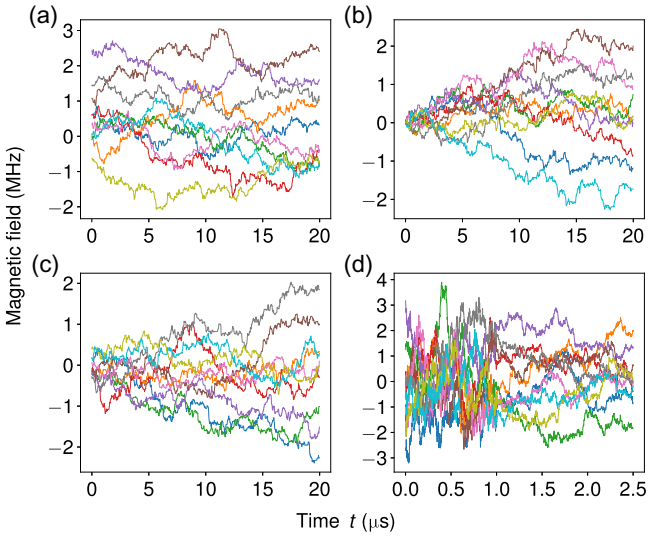

FIG. 8. Simulation of the magnetic field as a function of time for ten trajectories of Markovian noise with standard deviation of 1.2 MHz and correlation time $t_c = 42$ μs (a) at equilibrium, (b) quenched, and (c) quenched with a delay t_d of 2.5 μs, and (d) ten trajectories of Markovian noise with standard deviation of 1.2 MHz and a correlation time t_c that switches abruptly from 200 ns to 2 μs at $t_s = 1$ μs.

with probability $p_{\text{ret}} = e^{\frac{-\Delta t}{t_c}}$ or sample a new value from $N(0, \Delta_M)$ with probability $1 - p_{\text{ret}} = 1 - e^{\frac{-\Delta t}{t_c}}$. This produces a sequence of $t_{\text{total}}/\Delta t$ values, but this sequence will not represent continuous noise—rather, it will have large jumps roughly every $t_c/\Delta t$ points. To produce continuous equilibrium Markovian noise with the desired parameters, we average $M = t_c/\Delta t$ of these sequences, setting $\Delta_M = \Delta\sqrt{M}$, so that the noise will change by a small amount (roughly $\Delta\sqrt{2/M}$) at every point, but the standard deviation at each point will be Δ, and the correlation time will be t_c, as desired. An example of equilibrium Markovian noise generated with this method is shown in Fig. 8(a). In our experiment, the temporal resolution is set by the pulser clock, with a discretization step of $\Delta t = 4$ ns. The noise realizations are implemented electronically with the use of a Quantum Machines OPX controller, which orchestrates and synchronizes the full experimental sequence—triggering the laser and microwave pulses and reading out the transistor-transistor logic signals from single-photon-counting modules (avalanche photodiodes). The experimental setup is described in detail in Ref. [69].

For the quenched experiments, the quench is implemented digitally at the waveform-generation stage. Each stochastic sequence is produced with the required initial conditions—$n(0) = 0$ for Markovian quenches and $n(0) = n'(0) = 0$ for non-Markovian quenches—and uploaded to the OPX arbitrary waveform generator. The OPX controller synchronizes the start of the noise waveform with the first $\pi/2$ pulse of the Ramsey sequence, ensuring that the quench onset coincides with the beginning of the sensor's free-evolution period. The effective timing resolution of the noise control is 1–4 ns, much shorter than any correlation times t_c explored experimentally, thereby guaranteeing that the quench dynamics are well-resolved relative to the bath timescales.

A modification of this procedure can be used to generate quenched Markovian noise. As shown in Appendix A 1, quenched Markovian noise, which has the initial condition $n(0) = 0$, has an extra term in the correlation function corresponding to the dissipation of this quench as the system returns to equilibrium. The effect of this term is that the variance of the noise will change for each time point, so the variance $\sigma(t)^2$ of the normal distribution from which we sample must also change. From the correlation function $\langle n(t_1)n(t_2)\rangle = \Delta^2\left(e^{\frac{-|t_1-t_2|}{t_c}} - e^{\frac{-(t_1+t_2)}{t_c}}\right)$, we have the condition

$$\begin{aligned}\langle n(t)\, n(t+\Delta t)\rangle &= \Delta^2\left(e^{\frac{-\Delta t}{t_c}} - e^{\frac{-(2t+\Delta t)}{t_c}}\right)\\ &= e^{\frac{-\Delta t}{t_c}}\,\langle n(t)\, n(t)\rangle\\ &= p_{\text{ret}}\,\langle n(t)\, n(t)\rangle\,, \end{aligned} \tag{E1}$$

so $p_{\text{ret}} = e^{\frac{-\Delta t}{t_c}}$, as before, and we also have the condition

$$\begin{aligned}\langle n(t+\Delta t)\, n(t+\Delta t)\rangle &= \Delta^2\left(1 - e^{\frac{-2(t+\Delta t)}{t_c}}\right)\\ &= p_{\text{ret}}\,\langle n(t)\, n(t)\rangle\\ &\quad + (1-p_{\text{ret}})\sigma(t+\Delta t)^2, \end{aligned} \tag{E2}$$

which gives $\sigma(t+\Delta t) = \Delta\sqrt{1 - e^{\frac{-(2t+\Delta t)}{t_c}}}$. Because $\frac{\langle n(t)n(t+\Delta t)\rangle}{\langle n(t)n(t)\rangle}$ is independent of t, these same conditions apply for all time points. Thus, to generate quenched Markovian noise, we follow the same procedure as for equilibrium Markovian noise, averaging $M = t_c/\Delta t$ sequences, but with the modification that the first point of each sequence is always initialized to be 0, and for subsequent points, we either retain the value of the previous point with probability $p_{\text{ret}} = e^{\frac{-\Delta t}{t_c}}$ or we sample a new value from $N(0, \sigma'_M(t))$, where $\sigma'_M(t) = \sigma_{\text{eq}}\sqrt{M}\sqrt{1 - e^{\frac{-(2t+\Delta t)}{t_c}}}$. An example of quenched Markovian noise generated with this method is shown in Fig. 8(b).

In addition to equilibrium and quenched Markovian noise, we also generate Markovian noise with a delayed quench and Markovian noise with a switched correlation time. To generate Markovian noise with a quench delay of t_d, we generate quenched Markovian noise for a series of time points $0, \Delta t, 2\Delta t, \ldots, t_{\text{total}} + t_d - \Delta t$ and discard the first $t_d/\Delta t$ time points. To generate Markovian noise with a correlation time that switches from t_a to t_b at some

time t_s, we generate equilibrium Markovian noise with a correlation time t_a for a series of time points 0, Δt, $2\Delta t, \ldots, t_s - \Delta t$, and then we change p_{ret} from $e^{\frac{-\Delta t}{t_a}}$ to $e^{\frac{-\Delta t}{t_b}}$ and continue generating noise for the rest of the time points t_s, $t_s + \Delta t$, $t_s + 2\Delta t, \ldots, t_{\text{total}} - \Delta t$. Examples of each of these types of noise are shown in Figs. 8(c) and 8(d).

b. Generation of underdamped non-Markovian noise trajectories

As discussed in Appendix A 2, the correlation function for non-Markovian ($m \neq 0$) noise is more complex than that for Markovian noise, so we cannot use the same strategy to generate non-Markovian noise directly. Instead, we first generate some approximation of white noise $\eta(t)$, and then numerically solve for the response of an underdamped harmonic oscillator to this noise to obtain the trajectory $n(t)$. We cannot reproduce the white noise correlation function $\langle \eta(t_1)\eta(t_2)\rangle = A\delta(t_1 - t_2)$ exactly, so instead, we produce Lorentzian noise with the correlation function $\langle \eta(t_1)\eta(t_2)\rangle = (A/\Delta t)e^{\frac{-|t_1-t_2|}{\Delta t}}$ for some Δt that will be sufficiently small so that the noise amplitude $n(t)$ we calculate at each point will not be affected much by the deviation from white noise. We then numerically obtain

$$n(t) - n_0(t) = \int_0^t \frac{1}{m\Omega} \sin(\Omega(t-s))e^{-\frac{t-s}{t_c}} \eta(s)\, ds \quad \text{(E3)}$$

for each time t as a Riemann sum with spacing Δt. For fully quenched non-Markovian noise, $n_0(t) = 0$, and this is exactly the desired trajectory $n(t)$ of the noise. For stationary non-Markovian noise, we also independently sample n_0' from the normal distribution $N(0, \omega_0\Delta)$ and n_0 from the normal distribution $N(0, \Delta)$, and then we compute $n_0(t)$ from Eq. (A7), and add it to the generated values of $n(t) - n_0(t)$ to give the trajectory $n(t)$ of the noise. Examples of equilibrium and quenched underdamped non-Markovian noise are shown in Fig. 9.

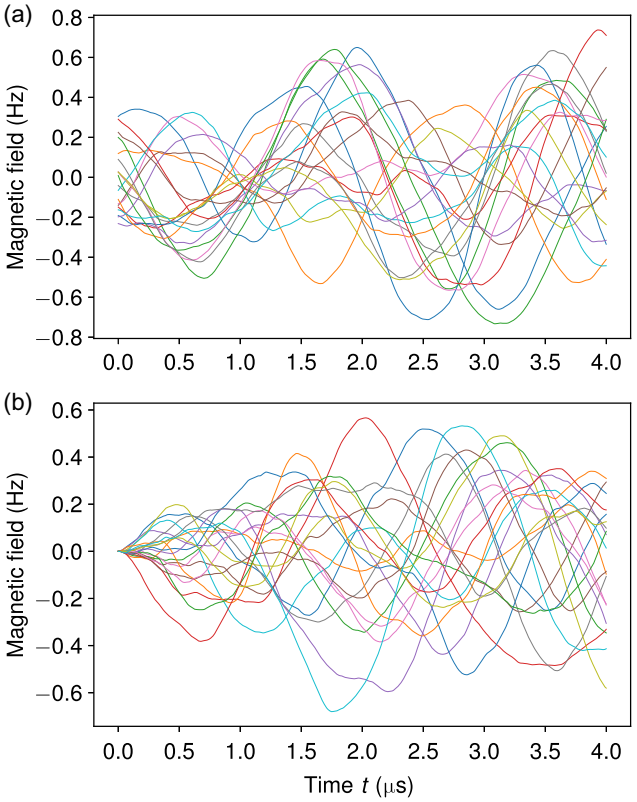

FIG. 9. Simulation of the magnetic field as a function of time for 20 trajectories of underdamped non-Markovian ($m \neq 0$) noise with driving strength $A/m^2 = 0.45 \times 10^{18}$ Hz^5, restoring frequency $\omega = 3$ MHz, and damping coefficient $\beta = 0.5$ MHz (a) at equilibrium and (b) quenched.

6. Procedure for Ramsey measurements in the innermost loop

For all of the measurements presented here, the 520 nm laser pulses have a power of 2 mW before the objective, and the Rabi driving power is 1.45 MHz. The Ramsey measurements in the innermost loop begin with a 3 μs pulse from the 520 nm laser to initialize the N-V center in the $|0\rangle$ state. Following this, a $\pi/2$ pulse is applied at the resonant frequency of the $|0\rangle \leftrightarrow |-1\rangle$ transition of the N-V center, after which the evolution time τ begins. During the evolution time, a noise trajectory of length τ is injected with use of the spiral under the diamond, and the state of the N-V center evolves to $|\psi\rangle_{t=\tau} = \frac{1}{\sqrt{2}}(|0\rangle + e^{i\varphi(\tau)}|-1\rangle)$, where $\varphi(\tau) = \gamma_{\text{N-}V}B_0\tau + \gamma_{\text{N-}V}\int_0^\tau \Delta B_z(t)dt$. Afterwards, a $-\pi/2$ pulse is applied to convert the phase into a population difference between the states, and then a 1.6 μs pulse from the 520 nm laser is applied. To maximize our ability to distinguish between the fluorescence of the $|0\rangle$ and $|-1\rangle$ states, we record the photon counts occurring between 220 and 400 μs after the start of the green laser pulse. We then carry out this sequence 4×10^5 times for each realization of the noise, as specified in Appendix E 4. Each Ramsey measurement in this innermost loop consists of two measurements, one with a $-\pi/2$ pulse in the rotating frame before the readout and one with a $\pi/2$ pulse, and the Ramsey decay curve is given by the normalized difference between the counts from these two sets of experiments, so the reported signal from the Ramsey measurement is given by $S(t) = (I_-(t) - I_+(t))/(\max(I_-(t) - I_+(t)))$, where $I_-(t)$ denotes the total counts measured for the Ramsey measurements with evolution time t and a $-\pi/2$ pulse before the readout, and $I_+(t)$ denotes the total counts measured for the Ramsey measurements with evolution time t and a $\pi/2$ pulse before the readout.

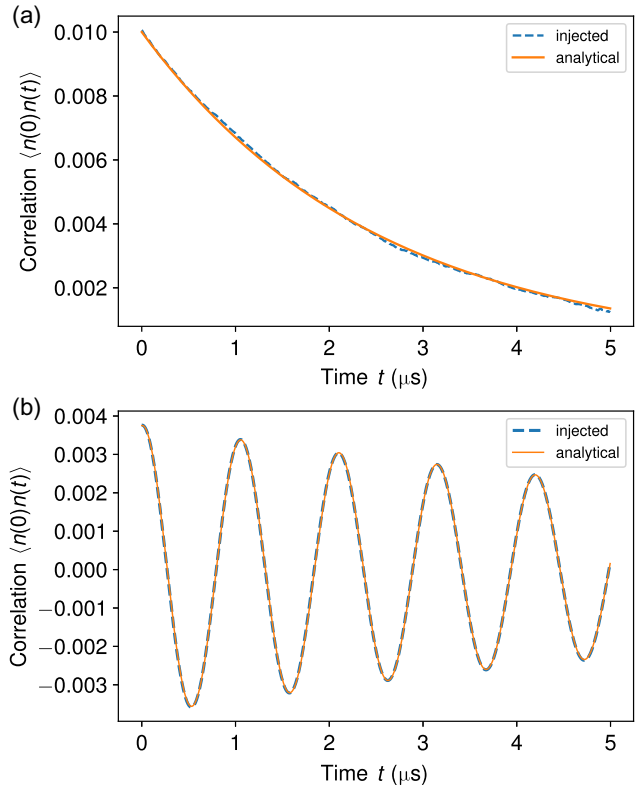

FIG. 10. Comparison of analytically predicted (solid lines) and empirically computed (symbols) correlation functions obtained from 10 000 realizations of (a) equilibrium Markovian noise with standard deviation $\Delta = 0.1$ V and correlation time $t_c = 2.5$ μs, and (b) equilibrium underdamped non-Markovian noise with driving strength $A/m^2 = 0.054$ V^2/μs^3, restoring frequency $\omega = 6$ MHz, and damping coefficient $\beta = 0.1$ MHz.

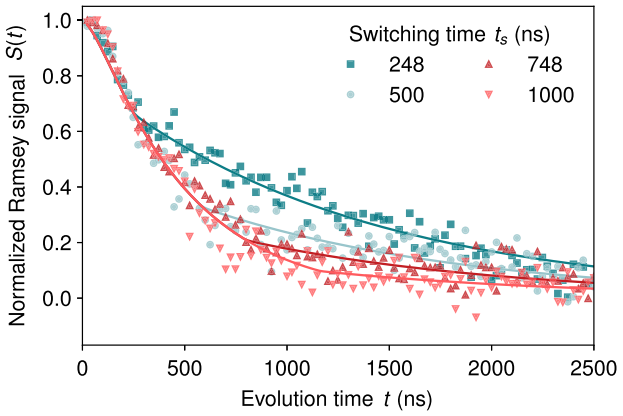

FIG. 11. Ramsey signals measured for equilibrium Markovian noise with a standard deviation of 0.10 V whose correlation time t_c switches from 75 ns to 15 ns at times t_s of 248, 500, 748, and 1000 ns.

APPENDIX F: VALIDATION OF INJECTED-NOISE CORRELATION FUNCTIONS

To verify how accurately the injected noise reproduces the intended correlation functions, we generated 10 000 realizations for each noise type—equilibrium Markovian noise and equilibrium underdamped non-Markovian noise—using typical experimental parameters. For each case, we computed the empirical correlation function $\langle n(0)n(t)\rangle$ by averaging the product $n(0)n(t)$ over realizations and compared it with the corresponding analytical prediction.

As shown in Fig. 10, the empirical correlation functions $\langle n(0)n(t)\rangle$ closely match the analytically predictions across the entire relevant time range. For the generation of underdamped non-Markovian noise, the sampling rate must satisfy $\Delta t \ll 2\pi/\Omega$ to ensure convergence in the Riemann-sum representation in Eq. (E3).

In our experiments, we use a discretization step of $\Delta t = 1$ ns for evaluation of this integral, which is well below $2\pi/\Omega$ and therefore sufficient to guarantee convergence for all injected underdamped non-Markovian noise samples. At substantially higher frequencies (e.g., Ω in the gigahertz range), achievement of convergence would require a finer discretization—i.e., a larger number of terms in the Riemann sum—leading to longer computation times.

APPENDIX G: AN ADDITIONAL EXAMPLE OF SWITCHED MARKOVIAN NOISE

We also measured Ramsey signals for equilibrium Markovian noise with a standard deviation of 0.10 V and a correlation time t_c that switches from 75 ns to 15 ns at times $t_s =$ of 248, 500, 748, and 1000 ns after the start of the measurement. The results are shown in Fig. 11, along with fits obtained with the analytical expression for the Ramsey signal of equilibrium Markovian noise with a switched correlation time derived in Appendix B 2, with the time of the switch relative to the start of the measurement as a free parameter. The switching times extracted from the fits are shown in Table IV, and match the known switching times used to generate the injected noise.

TABLE IV. Comparison of the switching times extracted from fitting the Ramsey signals in Fig. 11 with the analytical expressions vs the known values of the switching times for the injected noise.

Injected switching time t_s (ns)	248	500	748	1000
Fitted switching time t_s (ns)	239 ± 18	576 ± 29	790 ± 44	1150 ± 88

APPENDIX H: PARAMETER IDENTIFIABILITY AND COMPLEMENTARY REGIMES

The ability to extract all environmental parameters uniquely from experimental data depends on whether the measurement accesses the relevant dynamical regimes of the noise. In our framework, the parameters t_c, A/m^2, and ω_0 (or t_c and A/Γ^2 for Markovian noise) are formally independent. However, if the experiment probes only a restricted dynamical regime, the observable $\chi(t)$ may depend on specific parameter combinations, leading to apparent correlations in the fit. This is a universal feature of time-domain noise spectroscopy, not a peculiarity of our model.

For instance, in the stationary Markovian case, the short-time Ramsey attenuation depends only on the variance $\Delta^2 = \frac{1}{2} t_c A/\Gamma^2$, which combines t_c and A/Γ^2. Hence, experiments restricted to this regime cannot determine these two parameters independently. The introduction of a quench, however, modifies the short-time scaling to depend directly on A/Γ^2, thus providing an additional constraint that allows independent estimation of both t_c and A/Γ^2. This demonstrates how complementary stationary and quenched experiments provide full parameter identifiability.

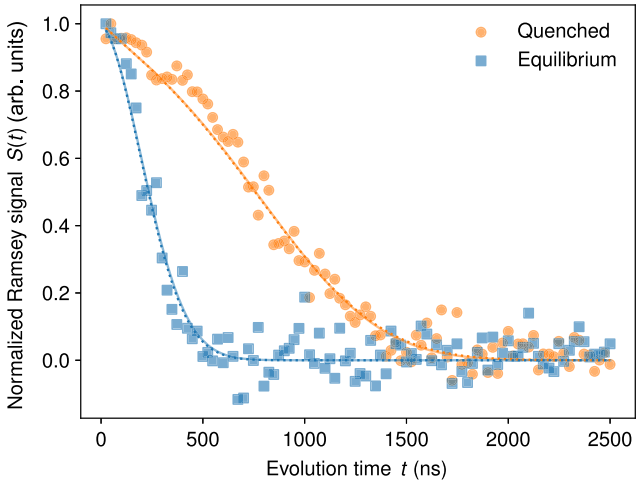

FIG. 12. Independent and joint fits of equilibrium (blue) and quenched (orange) Markovian noise with standard deviation $\Delta = 0.10\,\mathrm{V}$ and correlation time $t_c = 10\,\mu\mathrm{s}$. Transparent solid curves correspond to independent fits for each experiment. For the equilibrium case, the fit yields $t_c = 1000 \pm 1.69 \cdot 10^6\,\mu\mathrm{s}$, with $t_v = 0.000592$ [$P(> t_v) = 0.9995$, dependency of 0.9008], and for the quenched case, the fit yields $t_c = 106 \pm 1552\,\mu\mathrm{s}$, with $t_v = 0.0686$ [$P(> t_v) = 0.945$, dependency of 0.99999], neither of which is statistically significant, indicating that t_c alone has no measurable influence on the curves within this regime (t_v is Student's t score). Dotted curves show a global fit to both datasets, giving $t_c = 10.53 \pm 0.85\,\mu\mathrm{s}$, with $t_v = 12.33$ [$P(> t_v) < 0.00001$, dependency of 0.5048], a statistically significant result. The overlapping fitted curves demonstrate that both experiments are consistent with the same environmental parameters Δ and t_c. This comparison illustrates that a single experiment restricted to one dynamical regime cannot determine all noise parameters independently, whereas combining equilibrium and quenched measurements provides complete and unambiguous parameter estimation.

Figure 12 illustrates this principle for equilibrium and quenched Markovian noise. Independent fits to each curve are overparameterized, while a joint fit to both datasets recovers statistically meaningful and physically consistent values of t_c and Δ, confirming that combining different regimes resolves parameter correlations.

A similar reasoning extends to underdamped non-Markovian noise. In this regime, the environmental parameters influence the Ramsey response through distinct physical features: the short-time scaling of $\chi(t)$ encodes the noise strength A/m^2 (in a quenched experiment) and $\Delta^2 = A t_c/4\omega_0{}^2 m^2$ (in a stationary one), the frequency of oscillatory revivals reflects ω_0 in the underdamped regime, and their amplitude depends on t_c. Thus, by combining stationary and quenched experiments in the underdamped regime, one can disentangle A/m^2, ω_0, and t_c—parameters that may otherwise appear correlated when only a single regime is probed. This demonstrates the broader applicability of our framework for identifying and isolating environmental parameters across both Markovian and non-Markovian dynamics.

[1] A. Acín, I. Bloch, H. Buhrman, T. Calarco, C. Eichler, J. Eisert, D. Esteve, N. Gisin, S. J. Glaser, F. Jelezko, S. Kuhr, M. Lewenstein, M. F. Riedel, P. O. Schmidt, R. Thew, A. Wallraff, I. Walmsley, and F. K. Wilhelm, The quantum technologies roadmap: A European community view, New J. Phys. **20**, 080201 (2018).

[2] D. D. Awschalom, R. Hanson, J. Wrachtrup, and B. B. Zhou, Quantum technologies with optically interfaced solid-state spins, Nat. Photonics **12**, 516 (2018).

[3] I. H. Deutsch, Harnessing the power of the second quantum revolution, PRX Quantum **1**, 020101 (2020).

[4] W. H. Zurek, Decoherence, einselection, and the quantum origins of the classical, Rev. Mod. Phys. **75**, 715 (2003).

[5] K. Khodjasteh and L. Viola, Dynamically error-corrected gates for universal quantum computation, Phys. Rev. Lett. **102**, 080501 (2009).

[6] T. H. Taminiau, J. Cramer, T. van der Sar, V. V. Dobrovitski, and R. Hanson, Universal control and error correction in multi-qubit spin registers in diamond, Nat. Nanotechnol. **9**, 171 (2014).

[7] J. Zhang and D. Suter, Experimental protection of two-qubit quantum gates against environmental noise by dynamical decoupling, Phys. Rev. Lett. **115**, 110502 (2015).

[8] C. L. Degen, F. Reinhard, and P. Cappellaro, Quantum sensing, Rev. Mod. Phys. **89**, 035002 (2017).

[9] N. Aslam, H. Zhou, E. K. Urbach, M. J. Turner, R. L. Walsworth, M. D. Lukin, and H. Park, Quantum sensors for biomedical applications, Nat. Rev. Phys. **5**, 157 (2023).

[10] J. R. Maze, J. M. Taylor, and M. D. Lukin, Electron spin decoherence of single nitrogen-vacancy defects in diamond, Phys. Rev. B **78**, 094303 (2008).
[11] N. Zhao, S.-W. Ho, and R.-B. Liu, Decoherence and dynamical decoupling control of nitrogen vacancy center electron spins in nuclear spin baths, Phys. Rev. B **85**, 115303 (2012).
[12] A. Faribault and D. Schuricht, Spin decoherence due to a randomly fluctuating spin bath, Phys. Rev. B **88**, 085323 (2013).
[13] Z.-H. Wang and S. Takahashi, Spin decoherence and electron spin bath noise of a nitrogen-vacancy center in diamond, Phys. Rev. B **87**, 115122 (2013).
[14] H. Park, J. Lee, S. Han, S. Oh, and H. Seo, Decoherence of nitrogen-vacancy spin ensembles in a nitrogen electron-nuclear spin bath in diamond, npj Quantum Inf. **8**, 95 (2022).
[15] R. Hanson, L. P. Kouwenhoven, J. R. Petta, S. Tarucha, and L. M. K. Vandersypen, Spins in few-electron quantum dots, Rev. Mod. Phys. **79**, 1217 (2007).
[16] R. W. Simmonds, K. M. Lang, D. A. Hite, S. Nam, D. P. Pappas, and J. M. Martinis, Decoherence in Josephson phase qubits from junction resonators, Phys. Rev. Lett. **93**, 077003 (2004).
[17] B. E. Kane, A silicon-based nuclear spin quantum computer, Nature **393**, 133 (1998).
[18] K. Khodjasteh and D. A. Lidar, Fault-tolerant quantum dynamical decoupling, Phys. Rev. Lett. **95**, 180501 (2005).
[19] G. S. Uhrig, Keeping a quantum bit alive by optimized π-pulse sequences, Phys. Rev. Lett. **98**, 100504 (2007).
[20] J. Du, X. Rong, N. Zhao, Y. Wang, J. Yang, and R. B. Liu, Preserving electron spin coherence in solids by optimal dynamical decoupling, Nature **461**, 1265 (2009).
[21] A. M. Souza, G. A. Álvarez, and D. Suter, Robust dynamical decoupling for quantum computing and quantum memory, Phys. Rev. Lett. **106**, 240501 (2011).
[22] D. Suter and G. A. Álvarez, Colloquium: Protecting quantum information against environmental noise, Rev. Mod. Phys. **88**, 041001 (2016).
[23] G. A. Álvarez, A. Ajoy, X. Peng, and D. Suter, Performance comparison of dynamical decoupling sequences for a qubit in a rapidly fluctuating spin bath, Phys. Rev. A **82**, 042306 (2010).
[24] J. Clausen, G. Bensky, and G. Kurizki, Bath-optimized minimal-energy protection of quantum operations from decoherence, Phys. Rev. Lett. **104**, 040401 (2010).
[25] G. A. Álvarez and D. Suter, Measuring the spectrum of colored noise by dynamical decoupling, Phys. Rev. Lett. **107**, 230501 (2011).
[26] N. Bar-Gill, L. Pham, C. Belthangady, D. Le Sage, P. Cappellaro, J. Maze, M. Lukin, A. Yacoby, and R. Walsworth, Suppression of spin-bath dynamics for improved coherence of multi-spin-qubit systems, Nat. Commun. **3**, 858 (2012).
[27] F. K. Malinowski, F. Martins, P. D. Nissen, E. Barnes, Ł. Cywiński, M. S. Rudner, S. Fallahi, G. C. Gardner, M. J. Manfra, C. M. Marcus, and F. Kuemmeth, Notch filtering the nuclear environment of a spin qubit, Nat. Nanotechnol. **12**, 16 (2017).
[28] J. Bylander, S. Gustavsson, F. Yan, F. Yoshihara, K. Harrabi, G. Fitch, D. G. Cory, Y. Nakamura, J.-S. Tsai, and W. D. Oliver, Noise spectroscopy through dynamical decoupling with a superconducting flux qubit, Nat. Phys. **7**, 565 (2011).
[29] Y. Sung, F. Beaudoin, L. M. Norris, F. Yan, D. K. Kim, J. Y. Qiu, U. von Lüpke, J. L. Yoder, T. P. Orlando, S. Gustavsson, L. Viola, and W. D. Oliver, Non-Gaussian noise spectroscopy with a superconducting qubit sensor, Nat. Commun. **10**, 3715 (2019).
[30] D. F. Wise, J. J. L. Morton, and S. Dhomkar, Using deep learning to understand and mitigate the qubit noise environment, PRX Quantum **2**, 010316 (2021).
[31] A. Zwick, G. A. Álvarez, and G. Kurizki, Maximizing information on the environment by dynamically controlled qubit probes, Phys. Rev. Appl. **5**, 014007 (2016).
[32] J. F. Barry, J. M. Schloss, E. Bauch, M. J. Turner, C. A. Hart, L. M. Pham, and R. L. Walsworth, Sensitivity optimization for NV-diamond magnetometry, Rev. Mod. Phys. **92**, 015004 (2020).
[33] R. Budakian *et al.*, Roadmap on nanoscale magnetic resonance imaging, Nanotechnology **35**, 412001 (2024).
[34] E. Janitz, K. Herb, L. A. Völker, W. S. Huxter, C. L. Degen, and J. M. Abendroth, Diamond surface engineering for molecular sensing with nitrogen–vacancy centers, J. Mater. Chem. C **10**, 13533 (2022).
[35] D. Yudilevich, R. Stöhr, A. Denisenko, and A. Finkler, Mapping single electron spins with magnetic tomography, Phys. Rev. Appl. **18**, 054016 (2022).
[36] B. L. Dwyer, L. V. H. Rodgers, E. K. Urbach, D. Bluvstein, S. Sangtawesin, H. Zhou, Y. Nassab, M. Fitzpatrick, Z. Yuan, K. De Greve, E. L. Peterson, H. Knowles, T. Sumarac, J.-P. Chou, A. Gali, V. V. Dobrovitski, M. D. Lukin, and N. P. de Leon, Probing spin dynamics on diamond surfaces using a single quantum sensor, PRX Quantum **3**, 040328 (2022).
[37] K. S. Liu, A. Henning, M. W. Heindl, R. D. Allert, J. D. Bartl, I. D. Sharp, R. Rizzato, and D. B. Bucher, Surface NMR using quantum sensors in diamond, Proc. Natl. Acad. Sci. **119**, e2111607119 (2022).
[38] G. A. Álvarez, D. Suter, and R. Kaiser, Localization-delocalization transition in the dynamics of dipolar-coupled nuclear spins, Science **349**, 846 (2015).
[39] Y. Li, T.-G. Zhou, Z. Wu, P. Peng, S. Zhang, R. Fu, R. Zhang, W. Zheng, P. Zhang, H. Zhai *et al.*, Emergent universal quench dynamics in randomly interacting spin models, Nat. Phys. **20**, 1966 (2024).
[40] Y.-X. Wang and A. A. Clerk, Intrinsic and induced quantum quenches for enhancing qubit-based quantum noise spectroscopy, Nat. Commun. **12**, 6528 (2021).
[41] A. Norambuena, J. R. Maze, P. Rabl, and R. Coto, Quantifying phonon-induced non-Markovianity in color centers in diamond, Phys. Rev. A **101**, 022110 (2020).
[42] P. Kairys, J. C. Marcks, N. Delegan, J. Zhang, D. D. Awschalom, and F. J. Heremans, Quantifying the limits of controllability for the nitrogen-vacancy electron spin defect, arXiv:2309.03120.
[43] P. Penshin, T. Amro, T. Zabelotsky, A. Abramovich, T. Pandit, K. I. O. Ben'Attar, A. Hen, R. Uzdin, and N. Bar-Gill, Realization of robust quantum noise characterization in the presence of coherent errors, AVS Quantum Sci. **6**, 025002 (2024).

[44] F. Ginot, J. Caspers, M. Krüger, and C. Bechinger, Barrier crossing in a viscoelastic bath, Phys. Rev. Lett. **128**, 028001 (2022).
[45] F. D. Domínguez, M. C. Rodríguez, R. Kaiser, D. Suter, and G. A. Álvarez, Decoherence scaling transition in the dynamics of quantum information scrambling, Phys. Rev. A **104**, 012402 (2021).
[46] P. C. Jerger, Y.-X. Wang, M. Onizhuk, B. S. Soloway, M. T. Solomon, C. Egerstrom, F. J. Heremans, G. Galli, A. A. Clerk, and D. D. Awschalom, Detecting spin-bath polarization with quantum quench phase shifts of single spins in diamond, PRX Quantum **4**, 040315 (2023).
[47] A. Polkovnikov, K. Sengupta, A. Silva, and M. Vengalattore, Colloquium: Nonequilibrium dynamics of closed interacting quantum systems, Rev. Mod. Phys. **83**, 863 (2011).
[48] R. J. Lewis-Swan, A. Safavi-Naini, A. M. Kaufman, and A. M. Rey, Dynamics of quantum information, Nat. Rev. Phys. **1**, 627 (2019).
[49] M. Ban, Decoherence of qubit entanglement caused by transient environments, J. Phys. B: At. Mol. Opt. Phys. **40**, 689 (2007).
[50] C. Booker, B. Buča, and D. Jaksch, Non-stationarity and dissipative time crystals: spectral properties and finite-size effects, New J. Phys. **22**, 085007 (2020).
[51] A. Basit, H. Ali, F. Badshah, X.-F. Yang, and G.-Q. Ge, Controlling sudden transition from classical to quantum decoherence via non-equilibrium environments, New J. Phys. **22**, 033039 (2020).
[52] M. Kuffer, A. Zwick, and G. A. Álvarez, Path integral framework for characterizing and controlling decoherence induced by nonstationary environments on a quantum probe, PRX Quantum **3**, 020321 (2022).
[53] M. Kuffer, A. Zwick, and G. A. Álvarez, Sensing out-of-equilibrium and quantum non-Gaussian environments via induced time-reversal symmetry breaking on the quantum-probe dynamics, PRX Quantum **6**, 020320 (2025).
[54] M. M. Wolf, J. Eisert, T. S. Cubitt, and J. I. Cirac, Assessing non-Markovian quantum dynamics, Phys. Rev. Lett. **101**, 150402 (2008).
[55] W. Cui, Z. R. Xi, and Y. Pan, Optimal decoherence control in non-Markovian open dissipative quantum systems, Phys. Rev. A **77**, 032117 (2008).
[56] B.-H. Liu, L. Li, Y.-F. Huang, C.-F. Li, G.-C. Guo, E.-M. Laine, H.-P. Breuer, and J. Piilo, Experimental control of the transition from Markovian to non-Markovian dynamics of open quantum systems, Nat. Phys. **7**, 931 (2011).
[57] Y. Guo, W. Ji, X. Kong, M. Wang, H. Sun, J. Zhou, Z. Chai, X. Rong, F. Shi, Y. Wang, and J. Du, Single-shot readout of a solid-state electron spin qutrit, Phys. Rev. Lett. **132**, 060601 (2024).
[58] M. W. Doherty, N. B. Manson, P. Delaney, F. Jelezko, J. Wrachtrup, and L. C. Hollenberg, The nitrogen-vacancy colour centre in diamond, Phys. Rep. **528**, 1 (2013).
[59] P. Szańkowski, G. Ramon, J. Krzywda, D. Kwiatkowski, and Ł. Cywiński, Environmental noise spectroscopy with qubits subjected to dynamical decoupling, J. Phys.: Condens. Matter **29**, 333001 (2017).
[60] J. F. Haase, P. J. Vetter, T. Unden, A. Smirne, J. Rosskopf, B. Naydenov, A. Stacey, F. Jelezko, M. B. Plenio, and S. F. Huelga, Controllable non-Markovianity for a spin qubit in diamond, Phys. Rev. Lett. **121**, 060401 (2018).
[61] G. A. Alvarez, E. P. Danieli, P. R. Levstein, and H. M. Pastawski, Environmentally induced quantum dynamical phase transition in the spin swapping operation, J. Chem. Phys. **124**, 194507 (2006).
[62] E. P. Danieli, G. A. Álvarez, P. R. Levstein, and H. M. Pastawski, Quantum dynamical phase transition in a system with many-body interactions, Solid State Commun. **141**, 422 (2007).
[63] M. E. Ziffer *et al.*, Quantum noise spectroscopy of criticality in an atomically thin magnet, arXiv:2407.05614.
[64] J. W. Rosenberg, M. Kuffer, I. Zohar, R. Stöhr, A. Denisenko, A. Zwick, and G. A. Alvarez, Data for: Witnessing non-stationary and non-Markovian environments with a quantum sensor, https://doi.org/10.34933/E08BE44A-98E7-4D1E-9FAF-D36205C1DD27.
[65] H.-P. Breuer and F. Petruccione, *The Theory of Open Quantum Systems* (Oxford University Press, Oxford, 2002).
[66] S. A. Momenzadeh, R. J. Stöhr, F. F. de Oliveira, A. Brunner, A. Denisenko, S. Yang, F. Reinhard, and J. Wrachtrup, Nanoengineered diamond waveguide as a robust bright platform for nanomagnetometry using shallow nitrogen vacancy centers, Nano Lett. **15**, 165 (2015).
[67] J. M. Binder, A. Stark, N. Tomek, J. Scheuer, F. Frank, K. D. Jahnke, C. Müller, S. Schmitt, M. H. Metsch, T. Unden, T. Gehring, A. Huck, U. L. Andersen, L. J. Rogers, and F. Jelezko, Qudi: A modular python suite for experiment control and data processing, SoftwareX **6**, 85 (2017).
[68] D. Yudilevich, A. Salhov, I. Schaefer, K. Herb, A. Retzker, and A. Finkler, Coherent manipulation of nuclear spins in the strong driving regime, New J. Phys. **25**, 113042 (2023).
[69] I. Zohar, B. Haylock, Y. Romach, M. J. Arshad, N. Halay, N. Drucker, R. Stöhr, A. Denisenko, Y. Cohen, C. Bonato, and A. Finkler, Real-time frequency estimation of a qubit without single-shot-readout, Quantum Sci. Technol. **8**, 035017 (2023).